EFFECTIVE CONNECTIVITY OF MOTOR NETWORK WITH TONGUE MOVEMENT

Author

Amnah Mahroo

NUST201463173MSMME62414F

Supervisor

Dr. Muhammad Nabeel Anwar

Department of Biomedical Engineering and Sciences

School of Mechanical and Manufacturing Engineering

National University of Sciences and Technology

H-12 Islamabad, Pakistan

August, 2017

EFFECTIVE CONNECTIVITY OF MOTOR NETWORK WITH TONGUE MOVEMENT

Author

AMNAH MAHROO

Registration Number

NUST201463173MSMME62414F

A thesis submitted in partial fulfillment of the requirement for the degree of
Masters of Sciences
In
Biomedical Sciences

Supervised by: **Dr. Muhammad Nabeel Anwar**

Thesis Supervisor's Signature: _____

Department of Biomedical Sciences and Engineering
School of Mechanical and Manufacturing Engineering
National University of Sciences and Technology
H-12 Islamabad, Pakistan
August, 2017

DECLARATION

I certify that this research work titled **"*Effective Connectivity of Motor Network with Tongue Movement*"** is my own work. The work has not been presented elsewhere for assessment. The material that has been used from other sources it has been properly acknowledged / referred.

_____

Amnah Mahroo

NUST201463173MSMME62414F

PLAGIARISM CERTIFICATE

(Turnitin Report)

This thesis has been checked for Plagiarism. Turnitin report endorsed by Supervisor is attached.

_____

Amnah Mahroo

NUST201463173MSMME62414F

Dr. Muhammad Nabeel Anwar

Signature: _____

Thesis Acceptance Certificate

It is certified that the final copy of MS Thesis written by **Amna Mahroo** (Registration No. **NUST201463173MSSMME62414F**), of SMME (School of Mechanical & Manufacturing Engineering) has been vetted by undersigned, found complete in all respects as per NUST statutes / regulations, is free of plagiarism, errors and mistakes and is accepted as partial fulfillment for award of MS/MPhil Degree. It is further certified that necessary amendments as pointed out by GEC members of the scholar have also been incorporated in this dissertation.

Signature:_____

Name of Supervisor: Dr. Muhammad Nabeel Anwar

Date:_____

Signature (HOD):_____

Date:_____

Signature (Principal):_____

Date:_____

COPYRIGHT STATEMENT

- Copyright in the text of this thesis rests with the student author. Copies (by any process) either in full, or of extracts, may be made only in accordance with instructions given by the author and lodged in the Library of NUST School of Mechanical & Manufacturing Engineering (SMME). Details may be obtained by the Librarian. This page must form part of any such copies made. Further copies (by any process) may not be made without the permission (in writing) of the author.
- The ownership of any intellectual property rights which may be described in this thesis is vested in NUST School of Mechanical & Manufacturing Engineering, subject to any prior agreement to the contrary, and may not be made available for use by third parties without the written permission of the SMME, which will prescribe the terms and conditions of any such agreement.
- Further information on the conditions under which disclosures and exploitation may take place is available from the Library of NUST School of Mechanical & Manufacturing Engineering, Islamabad.

ACKNOWLEDGEMENTS

All praise to Allah Almighty for bestowing me with the courage, knowledge and health to carry out this project. I am extremely thankful to my parents, Mr. and Mrs. Muhammad Tariq for their unconditional love and support. And how can I forget my loving husband, Muneeb Arshid, for motivating and encouraging me to pursue my education.

I would like to express my deepest gratitude to my supervisor, Dr. Muhammad Nabeel Anwar for having me as a graduate student. I remember starting this project with him from scratch and then complaining when things didn't work out as expected. We faced a few problems and delays but this project would not have been possible without his patience, immense support and guidance. My gratitude also goes to my co-supervisors, Zahra Fazal and Dr. Adeel Razi for providing their valuable time, advice and technical help regardless of their busy schedules.

I am also thankful to my project partner, my junior, Amna Malik. Thank you for running the uncountable DCM models for me, without your help this project would not have been completed timely. My lab members have always been a great support, I would also like to thank Aqsa, Ahmed, Atif, Ghina, Sidra and all the seniors and the juniors. Also, worth mentioning are my best friends, Misha and Fatima who made this three-year long journey bearable.

Lastly, my sincere regards to my GEC members, principal of SMME and administration for providing a great platform for carrying out research.

Amnah Mahroo

Dedicated to my beloved parents

Mr. & Mrs. Lt Col Muhammad Tariq

ABSTRACT

The purpose of this study was to investigate the interaction of the neural couplings underlying tongue movements with the movements of the hands and feet. We intend to explore whether the movement of the tongue differentially facilitates any of the upper or lower limb movements, since upper limbs are more frequently used in daily life. We examined the neural modulation of the motor network in 20 healthy subjects while they performed the motor task. The fMRI data of the motor task was downloaded from the human connectome project (HCP) database (https://db.humanconnectome.org/app/template/Login.vm). The motor task consisted of finger tapping, foot squeezing and horizontal and vertical movements of the tongue. Our study included 8 regions of interest consisting of right and left motor representations of the hands, feet and tongue along with the right and left hemispheric representations of the supplementary motor area (M1HL, M1HR, M1FL, M1FR, M1TL, M1TR, SMAL and SMAR). We used functional connectivity analysis and dynamic causal modeling to investigate the modulatory influence of regions of the tongue, hands and feet onto each other while the participants perform the tongue movements. The connectivity analysis showed that the M1 representations of hands and feet received strong inhibitory input from bilateral SMA during tongue movements. Furthermore, M1TL received strong excitatory input from both the contralateral and ipsilateral SMA, while M1TR received inhibitory input from contralateral while excitatory input from Ipsilateral SMA. Also, the backward connections from M1TL to SMA were excitatory while M1TR exerts inhibitory influence onto both the SMA. Moreover, the self-connections of M1TR were strongly inhibited while the self-connections of M1TL were excitatory. Our results indicate differential activation profiles of M1TL and M1TR, suggesting the motor control of the tongue are to be left

lateralized. Our effective connectivity results are consistent with the previous fMRI studies reporting lateralization of tongue movement.

Keywords: Neuroimaging, fMRI, effective connectivity, dynamic causal modeling, motor control

TABLE OF CONTENTS

LIST OF ACRONYMS

Bayesian Model Selection	BMS
Bayesian Parameter Averaging	BPA
Blood Oxygen Level Dependent	BOLD
Database	db
Dynamic Causal Modeling	DCM
Echo Time	TE
Echo-Planar Imaging	EPI
Electroencephalography	EEG
Family-wise Error	FWE
Fixed Effects	FFX
FMRIB Software Library	FSL
Full Width Half Maximum	FWHM
Functional Magnetic Resolution Imaging	fMRI
Gauss	G
General Linear Model	GLM
Hertz	Hz
Human Connectome Project	HCP
Magnetic Resolution Imaging	MRI
Magnetic Resonance	MR

Magnetic Resonance Spectroscopic Imaging	MRSI
Magnetoencephalography	MEG
Millimeter	mm
Minutes	min
Montreal Neurological Institute	MNI
Near Infrared Spectroscopy	NIRS
Positron Emission Tomography	PET
Potassium Ion	K^+
Premotor Cortex	PMC
Primary Motor Cortex	M1
Region of Interest	ROI
Repetition Time	TR
Seconds	s
Statistical Parametric Mapping	SPM
Supplementary Motor Area	SMA
Tesla	T

LIST OF FIGURES

LIST OF TABLES

Chapter 1

INTRODUCTION

The primary motor cortex (M1) consists of representations of the body parts somatotopically arranged with the well-defined local distribution of the tongue, arms and legs (Penfield & Boldrey, 1937; Volz, Eickhoff, Pool, Fink, & Grefkes, 2015). There are a number of brain areas involved in the motor preparation, planning and execution other than the M1 (Boudrias et al., 2012; Eickhoff & Grefkes, 2011; Volz et al., 2015). For example, simple movements of upper or lower limbs activate a distinct motor network consisting of bi-hemispheric areas including M1, supplementary motor area (SMA), premotor cortex, basal ganglia, cerebellum and somatosensory cortex (Grafton, Woods, & Mazziotta, 1993; Volz et al., 2015).

In a recent study, Volz et al. have suggested that due to the more frequent use of our hands in daily life activities as compared to the feet, the neural coupling underlying the movements of the upper limb are stronger and more lateralized as compared to the movements of the lower limb. Various studies have demonstrated the underlying inter-hemispheric lateralization for the movements of upper and lower limbs whereas studies investigating the motor voluntary control of the tongue, mouth, lip and jaws are scarce for fMRI mainly due to associated motion artifacts (Funk et al., 2008; Marquart, Birn, & Haughton, 2000). This is quite unfortunate considering the utility and importance of the tongue in daily life activities such as speaking, swallowing and the manipulation of food.

The understanding of tongue lateralized dominance for cortical representation is still unclear. Wildgruber et al. in 1996 reported strong bilateral activation in M1 during the vertical movements of the tongue, without any significant statistical lateralization. On the contrary, studies have also reported asymmetrical representation of the tongue in M1 with respect to the size of the activation as a result of performance of both the vertical and horizontal movements (Lotze, Seggewies, Erb, Grodd, & Birbaumer, 2000; Martin et al., 2004) albeit not reporting statistically significant significance (Funk et al., 2008).

1.1 Significance of the study

Dynamic causal modeling (DCM), a generic approach for inferring hidden (unobserved) neuronal states from measured brain. DCM was introduced in 2003 for fMRI data (Friston et al., 2003) and made available as open-source software within the Statistical Parametric Mapping (SPM) software.

At the time of writing, we didn't find any study related to the modulation of the motor network due to tongue movements using DCM. We intend to investigate whether modulation of the tongue influences the movement of the upper or lower limbs. We also examined the lateralization of motor control of the tongue movements using DCM to estimate effective connectivity within the motor network. We hypothesized that the movement of the tongue may differentially facilitate the movement of the upper or lower limbs.

1.2 Problem Statement

- Several diseases (i.e. stroke) cause motor impairments leading to disabilities of the upper and lower limbs and often the tongue as well

- It is not clear whether these motor regions influence (excite or inhibit) activity in each other
- The effective connectivity and underlying neuronal dynamics of the tongue movements within the motor cortex are still unknown

1.3 Objectives of the Study

The objectives of the study are as follows,

- To investigate the impact of the tongue movement on the motor network dynamics
- To apply effective connectivity analysis and dynamic causal modeling to investigate the lateralization of the tongue movement, as this has not been done before
- To investigate how tongue movements modulate the activity of limbs at the motor cortical level

Chapter 2

REVIEW OF LITERATURE

2.1 A brief overview of fMRI

Since 1895, when the concept of X-rays was introduced by Wilhelm Conrad Röntgen, its application in the field of magnetic resonance imaging (MRI) has proved to be the most significant imaging advancement (Logothetis, 2008). The history of magnetic resonance imaging includes many researchers, who have discovered NMR and described its underlying physics, but it is regarded to be invented by Paul C. Lauterbur in September 1971; who published the theory about it in March 1973. Later, in the 1980s, when MRI was used for the benefits of health and medicine, it quickly gained an unparalleled role in the field of diagnostics and basic research. Among the other vast ranges of benefits of MRI; in medicine, it can provide detailed insights of structural integration of organs, including the central nervous system. Also, it can be utilized to provide information related to tissue perfusion, vascularization and physiochemical changes taking place within the tissue. All these applications of MRI are well-recognized but in the 1990s, the introduction of functional MRI (fMRI) – the technique which measures the neural activity based on the hemodynamic changes – made a great impact on the progress of cognitive neuroscience research.

Nowadays, fMRI is extensively being used in humans to study the neural mechanisms controlling human actions and sensory processing. It is also being used to understand and conclude the cognitive aspects ranging from memory to recognition to social interactions to ethical behaviors. The immense research that has been done during the past two decades on

fMRI has made people fascinated that this technique could read human brains, which is highly criticized by both the scientific community and the public. fMRI and its related neuroimaging techniques can never read the mind of a person, nor are they meant to do so. Such techniques provide insights into the neuronal mechanism that contributes towards the understanding of how the human brain works. Numerous advantages of fMRI make this technique highly acceptable include its noninvasiveness, its comparatively good spatiotemporal resolution and its ability to invoke all the brain networks that are involved in a particular task (Logothetis, 2008).

2.1.1 Physics and the physiology

2.1.1.1 The Physics of MR signal

The underlying physics of MRI is based on the interaction of magnetic moments of the nuclei when the applied magnetic field gives rise to a phenomenon of magnetic resonance (Hashemi & Bradley). The atomic nuclei exhibiting nuclear spin may act as a simple magnetic dipole and achieve a high energy state by orienting against the applied magnetic field or display a low energy state by aligning in the direction of the applied magnetic field. Hence, the energy is absorbed or emitted in the range of radiofrequency while transiting between the two energy states.

The excited nucleus emits frequencies proportional to the magnetic field it experiences. The factor that determines the magnetic field that is possessed by the nucleus is the application of the strong magnetic field. As the phenomenon of the resonance frequency and magnetic field applied works differently for every nucleus, the programming of the imaging systems can be customized in a way to specifically detect the nuclei of interest. Nevertheless, the electrons surrounding the nucleus shield and modulate the magnetic field at the nucleus. These minor

differences are thus caused by the shielding effects on the resonance energy and are usually ignored in fMRI and conventional MR but form a basis in other spectroscopic methods of MR (Peter Jezzard, 2003).

2.1.1.2 The physiology of brain activation

Charles Sherrington, an English physiologist, demonstrated in 1890 that an increase in the blood flow occurs because of brain stimulation (Roy & Sherrington, 1890). It was also observed that the total oxygen supply exceeded the amount of oxygen being utilized, which is, the relative amount of oxygen present in the blood decreased. In 1992, Kuwabara et al. provided potential evidence of physiological importance that a working brain receives an increased rate of oxygen supply, but its rate of utilization may get limited because of the rate of oxygen exchange at the level of the capillaries (Buxton & Frank, 1997; Kuwabara, Ohta, Brust, Meyer, & Gjedde, 1992). The oxygen gradient between the mitochondria and the capillaries is achieved by enhancing the relative amount of oxygenated hemoglobin, hence compensating the rate of utilization. Thus, along with an increase in blood flow, a local increase in blood volume will also occur (Peter Jezzard, 2003).

Various aspects of the physiology of transfer of information in the brain such as the generation of electrical potential, increased glucose utilization (oxidative metabolism), relative oxygenation and increased local blood flow provide an underlying mechanism for various neuroimaging techniques. Functional magnetic resonance imaging is one of the modalities of neuroimaging which uses the changes in the blood flow and oxygenation for measuring brain activation.

2.1.2 Techniques for functional brain mapping

The methods of functional imaging explain the complex changes in a time course like that at which cognitive, motor or sensory processes occur. Precise interpretations require a method that is robust enough to localize the neuroanatomy of these complex changes. Hence, various functional imaging techniques are accordingly contrasted and compared to choose the best suited spatial and temporal resolution (Fig 2.1). Electrophysiological based methods, such as electroencephalography (EEG) detects the depolarization of neurons by directly mapping the generation of transient electrical dipoles or magnetic dipoles in the case of magnetoencephalography (MEG), in real time (10-100 msec), but these techniques have relatively poor spatial resolution (only a few mm-cm). On the contrary, positron emission tomography (PET) and functional neuroimaging (fMRI) detects the neuronal activation with relatively high spatial resolution (up to 1-10 mm) but have a limited temporal resolution as these techniques detect the much slower hemodynamic response generated because of the depolarization of neurons.

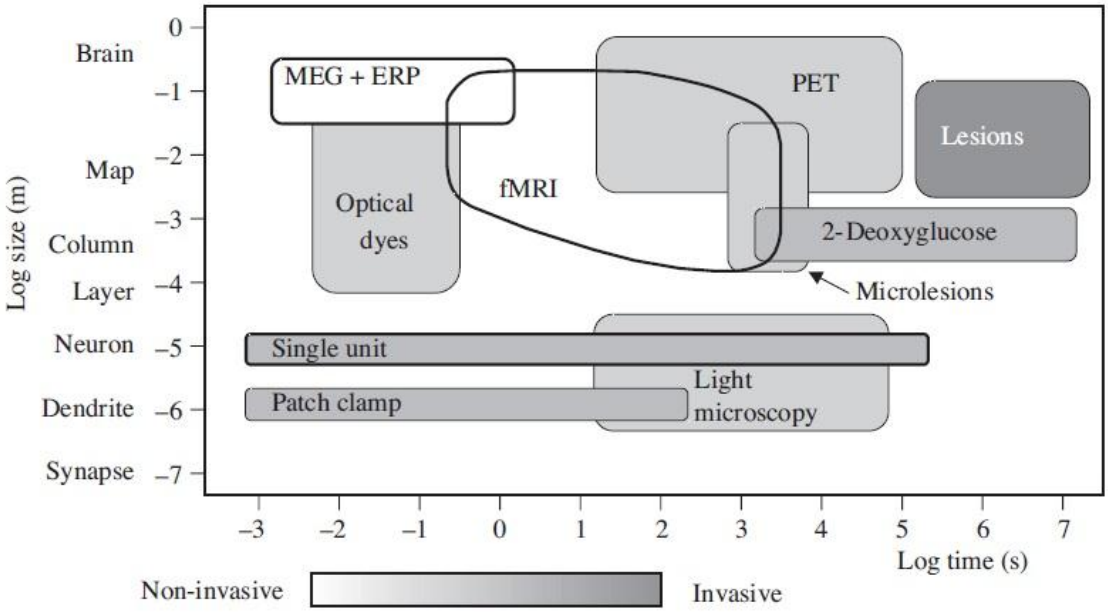

Figure 2.1: An illustrative comparison of functional brain imaging techniques. This is a popular version of illustration explaining temporal and spatial properties of different brain functional imaging techniques that can be applied on humans, animals or tissue preparations. fMRI has a unique link to high temporal and spatial resolution properties, providing a detailed understanding of neuronal organization of the brain (adapted from Cohen and Bookheimer 1994)

Other imaging techniques such as near infrared spectroscopy (NIRS) also measure changes in the blood flow at a cortical level but have low spatial resolution due to the scattering of light due to the presence of the skull. On the other hand, a relative benefit of fMRI and PET is that these techniques can have activations occurring in the deep brain areas as well. PET and other spectroscopic imaging techniques like magnetic resonance spectroscopic imaging (MRSI) can also detect neuronal activations deep in the brain, but their temporal and spatial resolution are compromised, mainly due to the chemical being used. Still, the information provided by these techniques is quite specific and complements the information provided by the fMRI (Peter Jezzard, 2003).

2.1.3 Principles of magnetic resonance imaging

Various methods can be used to detect functional activation of the brain such as, changes in the concentration of oxygen, blood volume, or by measurements of tissue perfusion. Currently, the center of attention for human neuroimaging is blood oxygen level dependent (BOLD) contrast (Logothetis, 2008; Ogawa & Lee, 1990; Ogawa, Lee, Nayak, & Glynn, 1990). The important advantages of using fMRI for investigating neuronal activations are the temporal and the spatial resolutions of the signal acquired. The temporal and spatial resolutions ensure our capability to discern the timings and the exact locations of the neuronal activations, respectively. The nature of the experimental design also critically affects the interpretability of the BOLD fMRI.

2.1.3.1 Spatial localization in MRI

The units used for measuring magnetic field strengths are usually Gauss (G) or Tesla (T). The imaging machine detects the location of resonating nuclei of small molecules present in the sample by using small gradients of magnetic fields in the range of 25-40 mT/m. This is then superimposed on a large static magnetic field with a strength of at least 1.5 T generated by the imaging magnet. The difference in the resonance frequency provides the measure to detect the relative positioning of the molecules present along the smaller gradient field, as the applied field strength is proportional to the resonance frequency of the nuclei present in the compound.

Advancements in the field of imaging has allowed researchers to extend this simple phenomenon of imaging in one dimension to two or three-dimensional multi-slice imaging by applying gradients along multiple directions. As the hemodynamic response lasts only a few seconds, and the switching of smaller magnetic fields previously took a lot of time, the

introduction of imaging techniques integrated with fast changing gradients made the use of fMRI more practical and robust, allowing researchers to acquire more images of the brain in a short period of time. One of these techniques is echo-planar imaging (EPI) (Mansfield, 1977), which is most popular nowadays, although several other techniques are also available.

2.1.3.2 Generation of contrast in MRI

The second major goal in imaging, other than spatial localization, is generating a contrast. When nuclear spins get excited from a low energy state to a high energy state, they can do the reverse, that is, they will get relaxed by emitting the energy absorbed, in the form of a radiofrequency as they move from a high energy state to a low energy state which will then be detected by the MRI. The interaction of spins with the environment surrounding them determines the efficiency of spin relaxation. This is called a lattice in physics terminology.

The rate constant which determines the time required to regain the magnetization has a value of $\frac{1}{T1}$ and T1 is known as the spin lattice relaxation time. Over a period of one T1, the excited spins revert to 66% of their magnetization and it takes three T1 cycles to regain 95% of the magnetization. Rapid applications of excitation pulses then allow for full relaxation which lowers the number of spins and ultimately results in a decreased resonance signal. This phenomenon provides the basis for generating an image contrast. The chemical environment surrounding the water molecule locally determines the T1 contrast. That is why the T1 contrast for a water molecule in the cerebrospinal fluid is much longer as compared to the tissue.

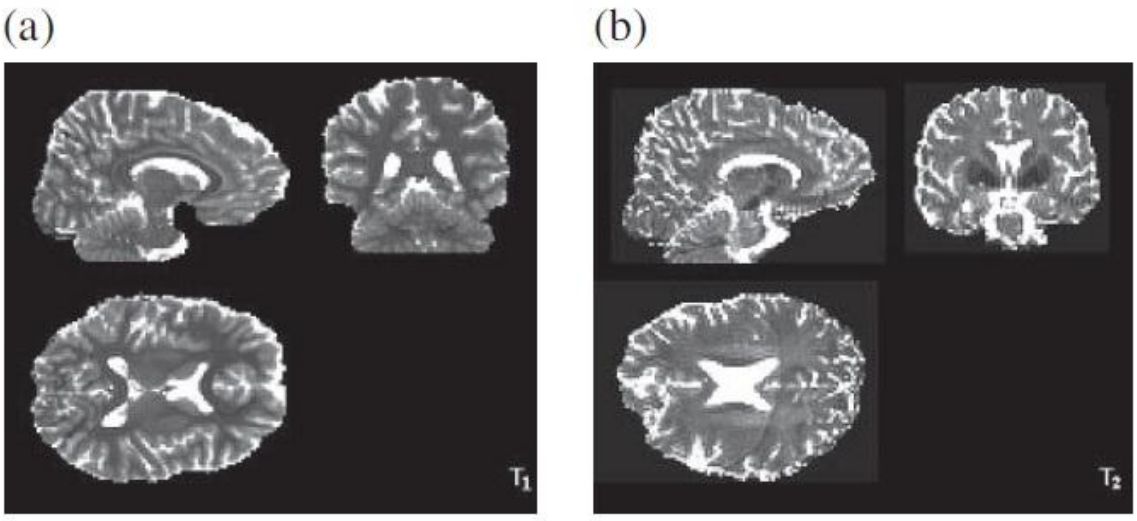

Figure 2.2: Demonstration of differences in T1 and T2 contrast images. The brain MRI contrast not only depends on the differences in the proton distribution in water and fat but is also influenced by the relaxation times. (a) Brain images demonstrated by differences in the T1 relaxation times. The lighter shades represent the longer T1 values. (b) Images on the right side represent the distribution of T2 relaxation time. As shown in the images, the tissue differences brought by T2 and T1 are not identical, irrespective of the fact that the water in the cerebrospinal fluid has longest values of T1 as well as T2. Variation in the pulse sequences are used to generate relative differences in T1 and T2 based on different types of tissue. Variations in the TE alter the relative relaxation time while a variation of TR interval alters the T1 contrast. (Adapted from the book Functional MRI: An introduction to Methods, Oxford University Press, USA, 2003)

As we decrease the 'TR' or the inter-pulse delay, by increasing the rate at which radiofrequency pluses are applied, the resonance signal acquired from the brain regions with shorter relative T1 relaxation times increase as compared to the regions which have a longer T1 (Fig 2.2). According to principle, if only a single molecule is being studied, it would follow the time constant T1 for its spin decay. The simple fact is that the molecule will emit energy if it is in an excited state. But, one sample consists of an enormous number of molecules exhibiting spins simultaneously.

At the level of a molecule, these nuclei happen to experience local and very small changes in the magnetic field. T1 relaxation is an exponential process. Whenever the magnetization vector is disturbed from its equilibrium value, the z-component of magnetization will recover in an exponential fashion, as shown in Fig 1.3. This plot shows the recovery of longitudinal magnetization with time for the case of zero magnetization at time t = 0. This is, for example, the case corresponding to the initial insertion of a sample into a static magnetic field.

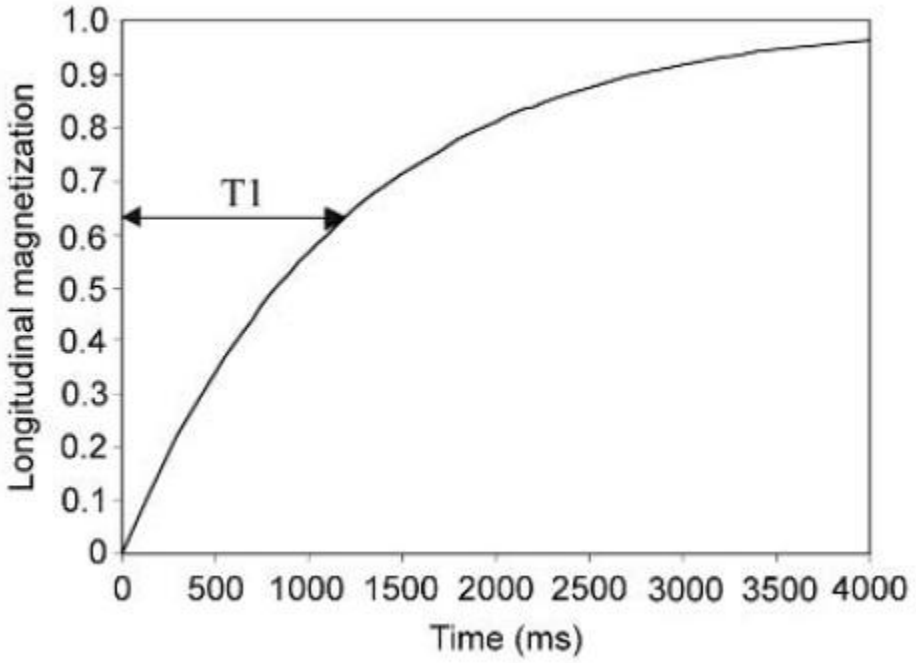

Figure 2.3: T1 relaxation curve. Recovery of longitudinal magnetization (Mz) following a 90° pulse. This is an exponential process, the time constant for which is described by the longitudinal relaxation time T1. The recovery curve for the case Mz (t = 0) is shown. (Adapted from the book Functional MRI: An introduction to Methods, Oxford University Press, USA, 2003)

Whereas T1 relaxation is a recovery process of longitudinal magnetization, T2 relaxation is a decay process of transverse magnetization. The T2 relaxation time is a measure of the rate of decay of transverse magnetization, and is also governed by an exponential process.

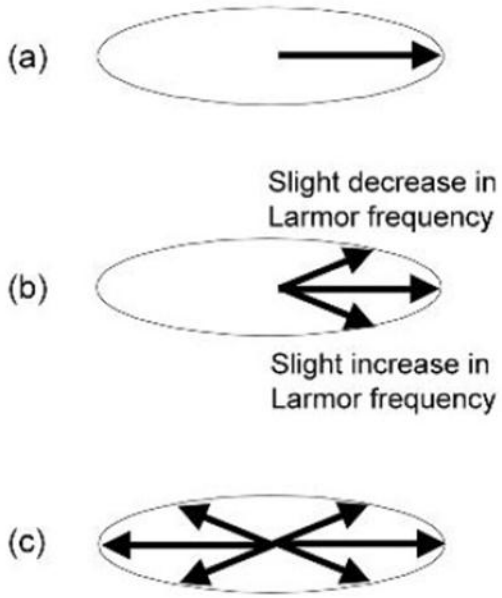

Figure 2.4: T2 Relaxation, the decay of transverse magnetization. (a) Initially, all the signals are in phase. (b) Random field fluctuations mean that some nuclei lag the system resonance frequency and some lead ahead. (c) Eventually, the spread of frequencies means that the signal is no longer coherently pointing along one direction and there is no signal detected (Adapted from the book Functional MRI: An introduction to Methods, Oxford University Press, USA, 2003).

An energy exchange occurs between the nuclei due to differences in the local magnetic field, thus, creating a loss in the phase coherence of their resonance emissions. The loss of coherence, in turn, causes a loss in the intensity of the total resonance signal summed from all the nuclei together, which is called T2 or spin-spin relaxation time, as shown in figure 1.4. In a specific chemical environment, the T2 is an inherent characteristic of the nuclei. By increasing T.E time, i.e., by lengthening the delay before the signal is detected in a pulse sequence, the signal acquired from the brain regions with a longer T2 for example, brain grey matter will relatively increase as compared to regions with shorter T2 such as brain white matter. In fMRI or

conventional MRI, the presence of protons in tissue water is of interest, instead of protons present in the fat.

Changes in the relative proportions of water protons allow contrast among brain structures. With the help of contrast, bone containing less water and hence generating a low MR signal can be distinguished from a higher MR generated signal from the brain as it contains more water. The local environments of water molecules affect the relaxation times of the proton nuclei which are utilized to develop further contrasts. Such contrast differences are generated by varying the mode in which spins are excited and detected by using pulse sequences.

Contrasts can be developed by varying three main parameters of pulse sequences. First is the flip angle which is the energy per pulse of radiofrequency energy. The more energy that is applied to the sample, the more time it takes to fully relax. Secondly, we can vary the rate of application of pulses. The rate is increased by decreasing the inter-pulse delay by shortening the TR (usually measured in seconds). The time allowed for T1 relaxation decreases as the TR decreases. Lastly, contrasts can be developed by changing the time delay before the signal is detected in the pulse sequence. That depends on the T.E time (usually measured in milliseconds). The higher the TE value, the less the signal is contributed by the nuclei having a shorter T2.

The signal decays at a faster rate if local field inhomogeneity is present which allows the molecules to diffuse through during the time period of a single TE. The movement of molecules into different magnetic fields caused by inhomogeneity slightly changes their resonance frequency, which then decreases the coherence of spins of the nuclei. The resulting net signal therefore decays more rapidly. The rate at which the signal decays due to the presence of inhomogeneities of local magnetic fields is represented by T2* relaxation time. This T2*

relaxation time is much shorter than the T2 in the brain areas where local magnetic fields change rapidly. Hence this can also be used as a basis for generating another contrast.

2.1.3.3 Mechanisms of haemodynamic change

When brain regions become active, the utilization of energy increases at the synapse and hence the local blood flow increases. (Duncan & Stumpf, 1991; Duncan, Stumpf, & Pilgrim, 1987) The precise details of mechanisms that cause metabolic changes are unclear. It has been suggested that the uptake of glutamate, the excitatory neurotransmitter by the adjacent astrocytes may be a major contributor to the increased utilization of energy (Magistretti & Pellerin, 1996). In the brain, astrocytes are present in a large quantity and exist adjacent to the neurons. Experiments using ^{13}C MRS have proposed that the glutamate keeps cycling between two cells, the neuron and the astrocyte as a result of oxidative glucose metabolism (Sibson et al., 1998).

However, it appears that the relationship between the increased blood flow and increased energy utilization is not so simple. The complexity arises when the mechanism of inhibition occurs at the synapse (Peter Jezzard, 2003). Theoretically, it is suggested that the release of inhibitory neurotransmitters may not lead to a substantial increase in the utilization of energy (Gjedde, 1997). Studies have shown that during a ‘go/no go’ motor paradigm or a simple ‘no go’ phase, the motor cortex does not show any detectable activations while inhibition of the motor cortex is demonstrated electrophysiologically (Rees, Friston, & Koch, 2000).

Nevertheless, as a general notion, other evidence does challenge this. In the motor cortex, the lateral superior olive has excitatory connections from the ipsilateral afferents, in contrast to the contralateral connections that are found to be inhibitory. It was shown that the stimulation of any of these two connections results in an increased uptake of deoxyglucose, which is an energy

utilization measure (Glendenning, Hutson, Nudo, & Masterton, 1985). Likewise, another study carried out in rats revealed that the stimulation of both, the parallel inhibitory fibers having di-synaptic connections and climbing excitatory fibers having mono-synaptic connections in the cerebellum leads to a local increase in blood flow (Mathiesen, Caesar, Akgoren, & Lauritzen, 1998). The changes in the blood flow in this system were directly correlated with the product of the magnitude of the magnetic field potentials and the frequencies of the stimulation, thus combining the effects of metabolic factors from both pre- and post-synaptic activity. It implies that more work is needed to clarify the interpretation of coupling the neuronal activity to the haemodynamic changes (Peter Jezzard, 2003).

The above mentioned observations have highlighted the key features of the fMRI BOLD response. It should be able to detect the changes based on the activation in the regions where synapses are present that are grey matter and not white matter. It should not directly measure the neuronal activity; instead the changes measured should represent synaptic activity or a combined effect of both the synaptic and electrical dendritic changes. Lastly, as excitatory synaptic activity triggers the cortical signal; the neuronal discharge rate should have a direct relationship with the magnitude of the BOLD response (Peter Jezzard, 2003; Rees et al., 2000).

2.1.3.4 Coupling of haemodynamic changes to neuronal activation

The underlying mechanisms that cause a local increase in the blood flow are still not fully understood. Several processes regulate the flow of blood to the brain. Myogenic, hormonal, and sympathetic mechanisms collectively regulate brain perfusion. More specific regulations are required to meet the changes in energy along with the brain activation. The factors that contribute local response include, release of K^+ due to neuronal depolarization, and the release of

adenosine and water in response to the unbalanced supply and utilization of oxygen. However, the most important chemical signal is the release of nitric oxide which occurs as a response to the local increases in blood flow due to the neuronal activation and is also an important indicator of hypercapnia in the cerebrum (Peter Jezzard, 2003).

Several circulating factors such as serotonin and norepinephrine as well as the locally released eicosanoids e.g., prostacyclin (Kuschinsky, 1991; Peter Jezzard, 2003) can modulate the flow of blood, as well as some of the drugs being commonly used (Dirnagl, Niwa, Lindauer, & Villringer, 1994; Ogawa et al., 1993). Studies have shown that age-dependent changes in the coupling between increased blood flow and neuronal activations may occur. For instance, in neonates, the concentration of deoxyhaemoglobin may relatively increase, instead of decreasing due to the activation of neuronal population (Meek et al., 1998). While the increase in blood flow due to neuronal activation may reduce with age. (Hock et al., 1995)

2.1.3.5 How is BOLD contrast generated?

In order to appreciate the phenomena of fMRI it is important to understand the BOLD response. The measure of change in the applied magnetic field when it gets in contact with a material, also known as magnetic susceptibility, forms the basis of BOLD fMRI.

Normally, blood is considered as a concentrated solution of haemoglobin, which acts as a diamagnetic when oxygen is bound to it, while it becomes paramagnetic when it loses oxygen (Pauling & Coryell, 1936). The diamagnetic materials have reduced magnetic flux, hence when magnetic field is applied it gets repelled. In contrast, the paramagnetic materials have high magnetic flux, so the applied magnetic field is attracted towards the material. Hence, the change in the oxygenation of the magnetic field may cause changes in the distortions of the applied

magnetic field. It has been demonstrated that the deoxygenation of haemoglobin causes the T2 relaxation time to vary exponentially (Thulborn, Waterton, Matthews, & Radda, 1982).

As the strength of the magnetic field increases, the change in the T2 relaxation time also increases as the difference in the magnetic susceptibility between the surrounding and the blood cells governs the phenomena. Ogawa (1990) showed a BOLD contrast image for the first time during a cat imaging experiment. The report from the experiment showed that when the cat was made hypoxic, the brain signal decreased around the blood vessels, while normoxia reverses this effect (Ogawa, Lee, Kay, & Tank, 1990). Magnetic susceptibility of blood vessels increases due to blood deoxygenation relative to the tissue surrounding the brain, giving rise to local field gradients and decreasing tissue T2* locally around the blood vessels in the tissue water. Later, Ogawa suggested that the small changes occurring in the brain due to neuronal activation can be imaged using this effect of relative oxygenation. In fact, the T2 changes characterized by the experiments of Thulborn and the T2* changes proposed by Ogawa explains distinct phenomena, though they are actually related (Peter Jezzard, 2003).

2.2 Brain Connectivity Analysis: An application of fMRI

A wide range of network analysis techniques may be applied and analyzed to study brain connectivity, several of which are applied in parallel or in conjunction of other techniques to describe and map other biological networks such as in ecology, gene regulation or cellular metabolism.

The theory of directed graphs which comes under the broad category of graph theory is of great importance as it can be applied to all levels of brain connectivity whether it is structural, functional or effective. Such graphs consist of vertices, which corresponds to the brain regions or

neurons, and edges, representing statistical dependencies, pathways or synapses between neural elements. Simply put, these graphs can be explained as a matrix of connections with binary elements showing the absence or presence of an edge between the vertices or brain regions. These vertices may have direct connections through which they interact or indirect links composed of multiple paths.

2.2.1 Functional and effective connectivity

Functional connectivity is an observable phenomenon which can be assessed using statistical dependencies, like transfer of entropy, coherence or correlations. On the contrary, effective connectivity uses an approach of constructing a model corresponding to the parameters and based on that, attempt to explain the dependencies observed in functional connectivity. Effective connectivity explains the causal or directed influence of coupling among various brain regions when a task is performed. Hence, it solely depends on the model constructed to explain that influence. It is considered crucial because the model comparison may limit the analysis, as comparison leads to selecting a model with the presence of specific brain connections, and thus inferences are drawn on only those specific connections. Each model in effective connectivity is used to explain an alternate hypothesis to explain the cause of observed data, hence recapitulating the scientific process (Friston, 2011).

Chapter 3

MATERIAL AND METHODS

3.1 Subjects

The HCP database is a big and reliable source of neuroimaging data. Recently, the HCP database has made public release of healthy human subjects for task fMRI, resting-state fMRI and structural data. Motor task data was downloaded using this link (https://db.humanconnectome.org/app/template/Login.vm). Twenty healthy subjects performed the motor task and their subsequent functional scans were acquired. The details of the inclusion and exclusion criteria can be found here (Van Essen et al., 2013; Van Essen et al., 2012). All the participants were between the ages of 22 and 35. The participants were excluded if they had any neurological, psychiatric or any other medical disorder which could affect brain processing.

3.2 Experimental design

The HCP motor task was adapted from the one structured by Buckner and colleagues (Buckner, Krienen, Castellanos, Diaz, & Yeo, 2011; Yeo et al., 2011).

Table 3.1 Parameters for HCP motor task

Parameters for HCP Motor task fMRI	
Frames per run	284
Run duration (min)	3:34
# of task blocks per run	10
Duration of task blocks (s)	12
Task cue at the start of block	Yes

Duration of task cue (s)	3

The participants were presented with visual cues and were asked to perform motor movements such as finger tapping of the right or left hand, squeezing their right or left toes, or moving their tongue to map the relevant motor areas in the brain. The cue was presented for 3s and each block consisted of 10 movements and lasted for 12s. Two runs were acquired and each of them consisted of 13 blocks, with 4 blocks for foot movements (2 left and 2 right), 4 for hand movements (2 left and 2 right), 2 for tongue movements and 3 fixation blocks (15s) per run. Table 1.0 shows the details of the experimental paradigm.

Five cue-paced (3s) movements (12s)

1. Left Foot
2. Right foot
3. Left Hand
4. Right Hand
5. Tongue

3.3 fMRI data processing

The HCP pipelines developed for data pre-processing are primarily based on FSL and FreeSurfer. The data acquired from the HCP db were also minimally preprocessed and further details of preprocessing can be acquired from HCP Volume pipeline (Glasser et al., 2013). The minimal preprocessing involves motion correction, gradient unwarping, EPI distortion

correction, brain-boundary-based registration of EPI to structural T1-weighted scan, non-linear (FNIRT) registration into MNI152 space, and grand-mean intensity normalization.

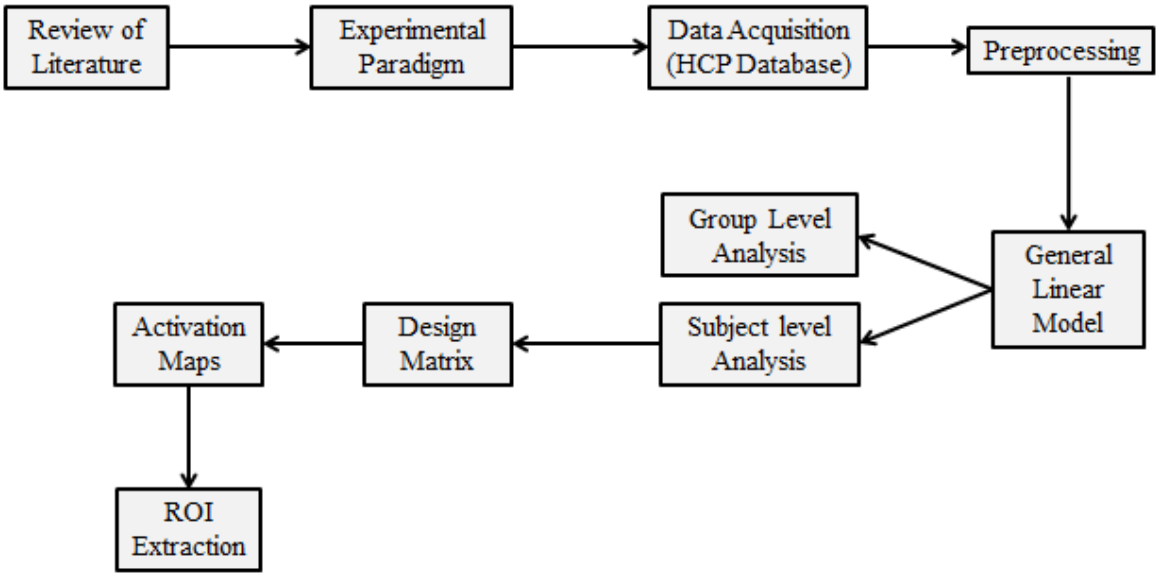

Figure 1.1: An overview of methodology. This figure represents a flow diagram of functional connectivity analysis, ending at the extraction of time series from the regions of interest (ROIs)

Additionally, the scans were smoothed using an isotropic smoothing kernel of 8 mm full width half maximum (FWHM). The low frequency drifts were removed by applying a high-pass filter of 1/128 Hz to the time series of each voxel.

3.3.1 GLM model design

Subject level analysis was carried out using SPM 12. The two runs were concatenated and first level GLM analysis was then applied. Five predictors were added into the model based on the motor movements which included the left foot, right foot, left hand, right hand and tongue. Each movement lasted for 12s and a 3s cue was presented before each block. Linear contrasts were generated based on this motor model and were used to develop motor activation

maps for each movement versus the baseline and versus all the other movements. Voxels which have t-values more than the height threshold of 5.11, with a p-value of 0.05 were considered significant (family-wise error (FWE) correction applied). The overview of the methodology is shown in Figure 1.1.

3.3.2 Dynamic causal modeling

Effective connectivity analysis was carried out using dynamic causal modeling (Friston, Harrison, & Penny, 2003) based on the bilinear state equation explained in Fig. 3.2. The coupling among the regions are estimated by DCM at the level of the neurons depending on three factors in the form of matrices, matrix (A) endogenous coupling (independent of task), matrix (B) task dependent coupling, and matrix (C) the direct input caused by experiment that drives the interregional coupling in the system (Volz et al., 2015). Figure 3.3 presents a schematic illustration of the steps involved in the analysis of DCM.

DCM estimates the rate at which neural activity change due to the influence of one brain area over another. DCM was applied at the subject level and the time series were extracted from 8 regions of interest (ROIs), adjusted for effects of interest at coordinates specific to the subjects. The ROIs, at a radius of 8mm, were defined as spheres centered upon individual activation maxima.

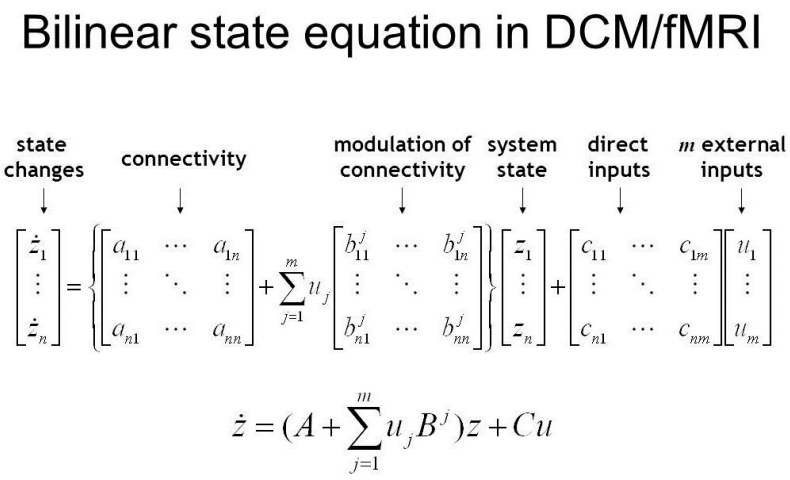

Figure 3.2: Bilinear state equation used in dynamic causal modeling in fMRI. The DCM matrix-A represents endogenous connectivity, matrix-B shows task induced modulation and matrix-C consists of direct input values (Adapted from the paper, Causal Modelling and Brain Connectivity in Functional Magnetic Resonance Imaging (Friston, 2009).

The regions of the motor network which are found active during isolated movements of the upper and lower limbs were extracted as ROIs (Grefkes, Eickhoff, Nowak, Dafotakis, & Fink, 2008; Kapreli et al., 2006; Luft et al., 2002). ROIs included the region of the primary motor cortex corresponding to the foot (M1foot) and hand (M1hand), ventrolateral premotor cortex (vPMC) and the supplementary motor area (SMA).

M1foot and M1hand in the left hemisphere were obtained using the contrasts 'right hand' and 'right foot' respectively, while the M1 ROIs in the right hemisphere were identified using the contrasts left foot and left hand. The unilateral simple movements of upper and lower limbs usually render reliable activations in the contralateral hemisphere of the brain (Volz et al., 2015). The premotor regions were extracted from the conjunction analysis of the right foot and right hand. This ensures that the premotor regions were involved in the movements of both the upper

and lower limbs. All ROIs were defined by the structural and anatomical criteria (Volz et al., 2015). For the DCM analysis we assumed that the premotor regions drive the neural activity in the network and thus were defined as input regions in DCM (Matrix C). The coordinates from the individual subjects are provided in Table 3.2.

Table 3.2: Individual fMRI activations used as ROIs for DCM

Subject	M1FR	M1FL	M1HR	M1HL	M1TR	M1TL	SMAR	SMAL	vPMCR	vPMCL
01	12,-40,68	-6,-46,68	46,-12,58	-42,-16,56	50,-8,28	-56,-6.26	2,2,60	0,-10,62	50,2,50	-46,0,50
02	2,-40,70	10,-44,76	42,-20,52	-40,-18,50	60,0,28	-60,-4,34	2,4,56	-2,-6,70	52,-8,40	-58,-20,44
03	4,-26,76	-8,-16,76	44,-16,62	-38,-18,62	52,-10,26	-54,-8,24	2,2,64	-6,-10,70	50,-6,52	-44,-4,54
04	8,-30,76	-4,-24,78	46,-18,62	-42,-22,62	58,-4,32	-58,-8,26	8,-4,66	-2,-6,62	44,-2,50	-52,-8,50
05	6,-28,76	-8,-14,78	40,-26,64	-40,-22,50	56,-4,24	-60,-6,20	2,16,56	-2,6,56	54,4,42	-40,-2,48
06	4,-16,74	-4,-16,76	46,-14,56	-32,-26,60	60,-2,34	-56,-4,28	0,-6,64	-2,-2,56	52,2,44	-54,-2,46
07	10,-38,78	-4,-14,76	32,-22,70	-40,-14,56	52,-8,32	-58,-4,38	4,4,56	-2,-8,56	56,2,44	-58,0,40
08	6,-30,76	-4,-22,74	44,-12,58	-42,-14,56	58,-4,32	-58,0,28	2,0,60	-2,-2,58	52,2,52	-44,-4,48
09	8,-28,76	-6,-34,74	40,-14,50	-42,-16,56	56,-6,26	-58,-4,40	10,-14,72	-2,-8,68	54,-2,42	-58,-2,38
10	12,-42,76	-6,-16,78	40,-22,64	-40,-24,56	62,4,32	-58,-4,38	4,6,64	-2,-10,56	58,2,38	-54,8,38
11	8,-28,76	-4,-22,70	46,-12,58	-44,-20,56	62,-2,30	-58,-6,38	0,-2,62	-4,-6,76	52,-32,28	-58,-4,38
12	12,-12,78	-4,-6,74	44,-14,56	-44,-20,56	58,-6,32	-60,6,32	0,10,56	-2,-6,68	62,6,22	-46,0,52
13	8,-18,68	-8,-28,56	42,-12,52	-40,-12,62	54,-8,32	-60,-2,26	6,-10,66	-4,4,56	44,,38,26	-52,-4,44
14	10,-48,72	-12,-40,78	40,-22,64	-52,-12,48	62,-2,24	-56,-6,22	2,-4,60	-4,-10,60	58,12,18	-58,-20,40
15	10,-38,76	-8,-42,76	52,-10,48	-42,-20,62	60,-4,20	-60,-6,18	0,-14,72	-10,-6,74	56,2,38	-52,6,40
16	18,-14,78	-4,-34,72	28,-16,72	-42,-22,52	58,-4,26	-58,8,20	4,6,68	-4,4,72	40,0,60	-46,0-54
17	4,-38,72	-4,--42,74	34,-24,50	-36,-22,66	62,-2,30	-62,-2,22	6,4,60	-2,-2,64	60,2,36	-52,0,36
18	4,-36,72	-6,-34,72	46,-14,58	-42,-20,62	56,-4,38	-52,-10,40	8,4 58	-4,-4,68	36,-4,46	-42,-6,62
19	2,-38,72	-6,-36,72	40,-22,64	-52,-32,52	60,-2,26	-58,0,34	4,12,50	-2,-6,58	54,0,42	-58,2,30
20	6,-26,78	-10,-42,76	40,-22,54	-44,-14,58	62,4,30	-56,-2,38	2,-4,72	-2,-8,60	56,-10,38	-52,0,38
Mean	8,-30,74	-6,-28,74	42,-16,58	-42,-18,56	58,-4,28	-58,-4,28	2,2,62	-2,-4,62	52,2,40	-52,-2,44
SD	4,10,3	2,12,5	5,5,6	4,5,5	4,4,4	2,3,7	3,8,6	2,5,6	6,12,10	5,7,6

3.3.2.1 Connectivity models

The anatomical connectivity data from the published studies was used to define the endogenous connections within the motor network (Volz et al., 2015). Hence, we supposed similar brain connections between the motor cortex and premotor regions. Fully connected endogenous connections were assumed between all the regions (Fig 3.4).

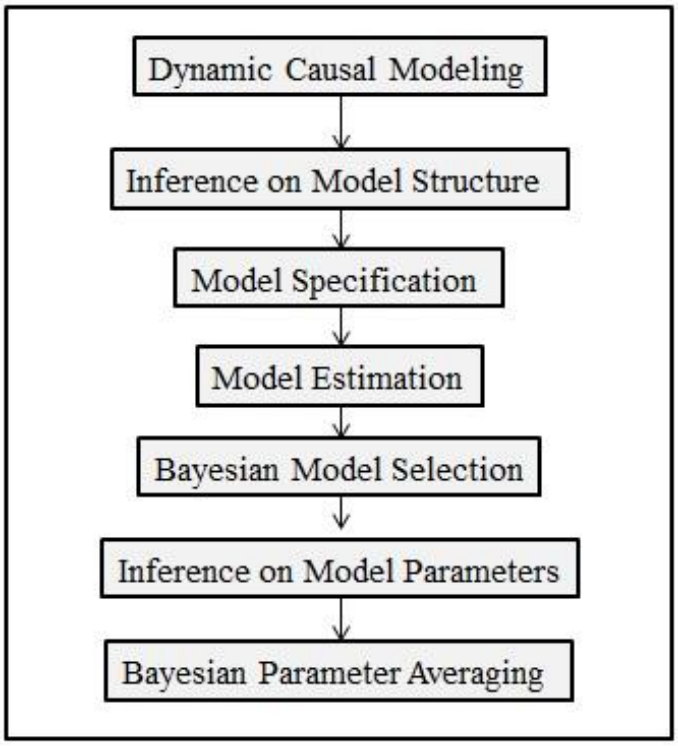

Figure 3.3: Schematic illustration for dynamic causal modeling. This figure shows the steps involved in the analysis of DCM.

SMA and contralateral and ipsilateral M1 (Rouiller et al., 1994), between SMA and contralateral (Boussaoud, Tanne-Gariepy, Wannier, & Rouiller, 2005) as well as ipsilateral vPMC (Luppino, Matelli, Camarda, & Rizzolatti, 1993), between vPMC and both contralateral and ipsilateral M1 (Rouiller et al., 1994), homotopic transcallosal connections among M1-M1

(Rouiller et al., 1994), vPMC-vPMC (Boussaoud et al., 2005), and SMA-SMA (McGuire, Bates, & Goldman-Rakic, 1991).

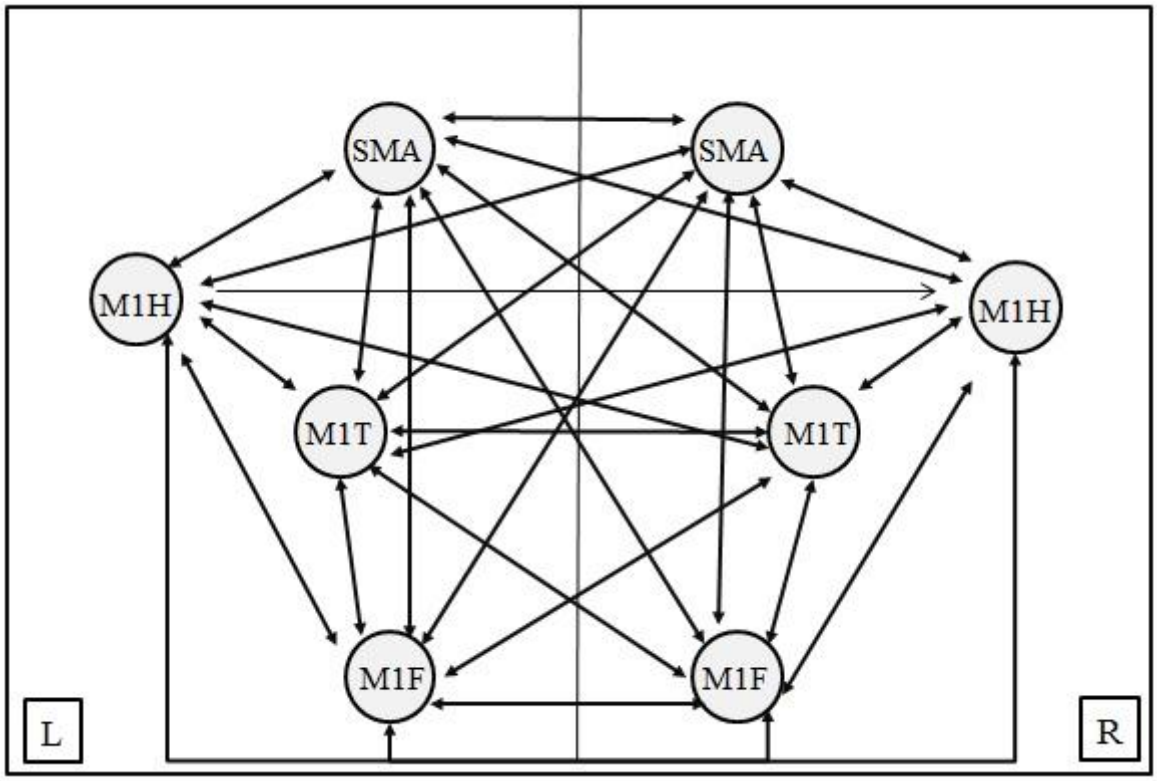

Figure 3.4: An illustration of endogenous connectivity represented by DCM matrix A. Fully connected matrix was assumed between all the regions for endogenous connections

We hypothesized four alternative models which can explain task specific modulation of coupling within the motor network. All the premotor regions (bilateral vPMC and the SMA) were defined as input regions in DCM in all the models (Matrix C) based on the assumption that motor tasks directly influence the activity of all premotor areas (Wang et al., 2011). Therefore, all models had some connections between the premotor regions and M1 contralateral to the movement. Moreover, as described in our hypothesis, we were particularly interested in the interaction between SMA and different M1 representations. Thus, the model 1 was constructed as the most sparse model with minimal number of connections. Model 1 is named as 'Ipsilateral

Connections' as it consisted of only ipsilateral bidirectional SMA connections with M1 representations of the hands, feet and tongue shown in Figure 3.5. Model 2 and 3 systematically varied in the number of connections modulated and in complexity. Model 2 was named as 'contralateral connections' as M1 representations of the hands, feet and tongue received SMA input only from the contralateral hemisphere (Fig 3.6). Model 3 was named as 'self-connections' because it was the only model that consisted of bilateral SMA connections with the M1 representations as well as self-connections of the tongue (M1TR and M1TL). Model 3 is shown in Figure 3.7. Lastly, model 4 was constructed as a fully connected model with 64 connections and hence was named as 'fully connected model' which is represented in Figure 3.8.

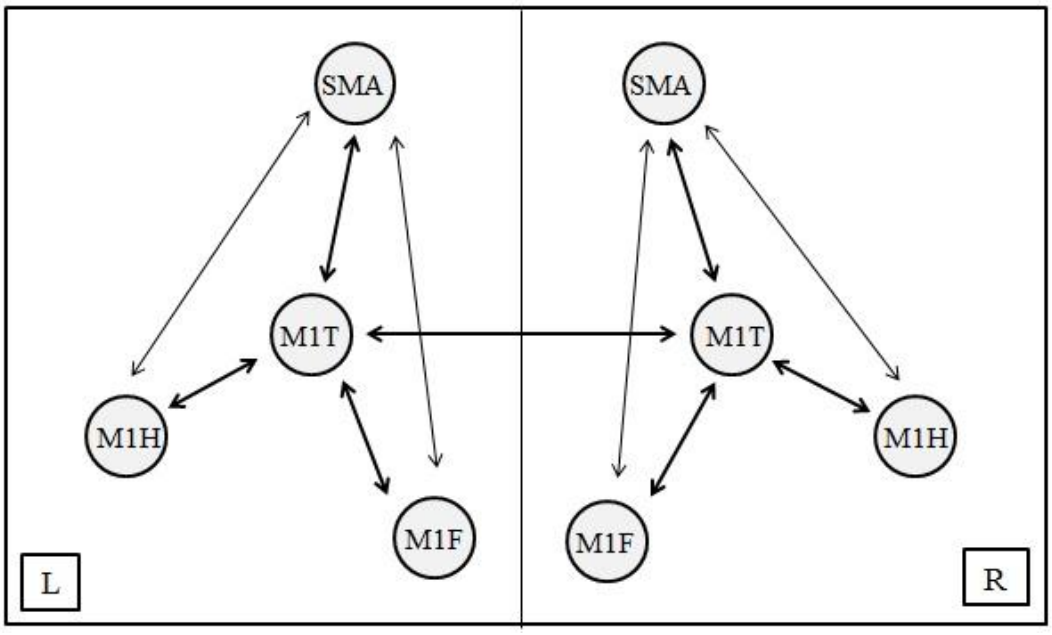

Figure 3.5: Demonstration of model 1. This model was named as the 'ipsilateral model' as it consists of Ipsilateral connections (within the same hemisphere) only among the M1 representations of the hands, feet, tongue and the SMA.

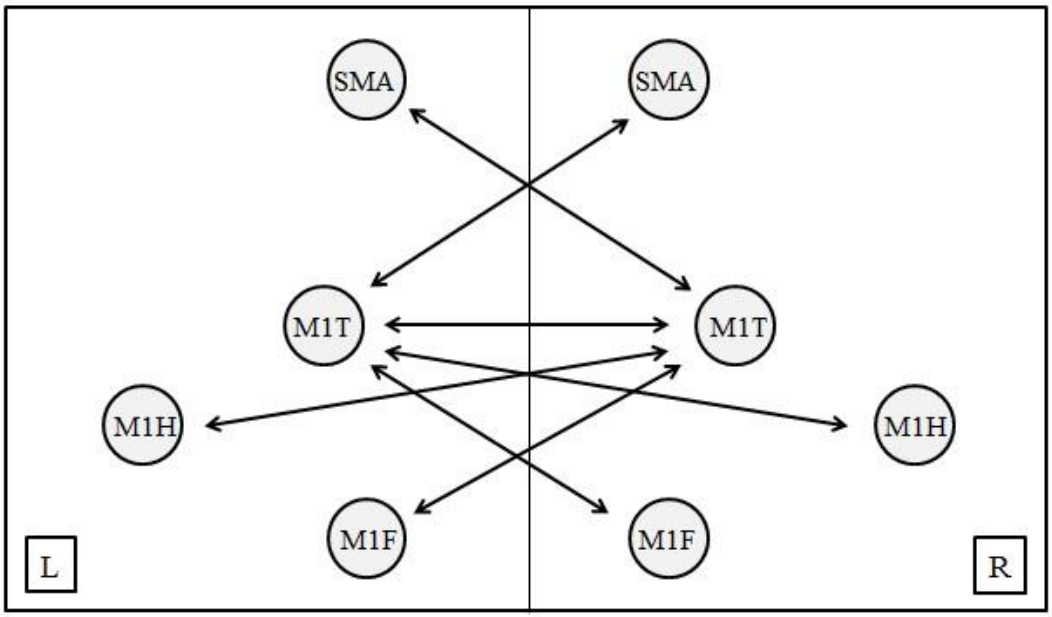

Figure 3.6: An illustration of Model 2. This model was named as the 'contralateral model' as shown by its name; it only consists of contralateral connections among the M1 representations of the movements and the SMA.

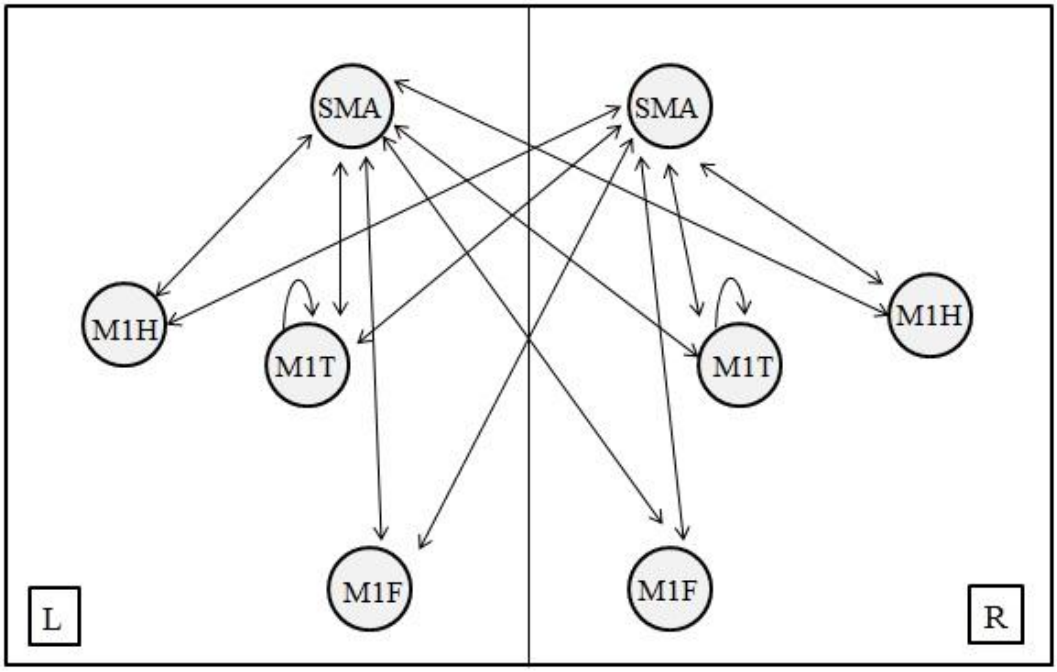

Figure 3.7: An illustration of model 3. This model was named as the 'self-connections model', as this was the only model which consisted of self-connections along with all the Ipsilateral and contralateral connections.

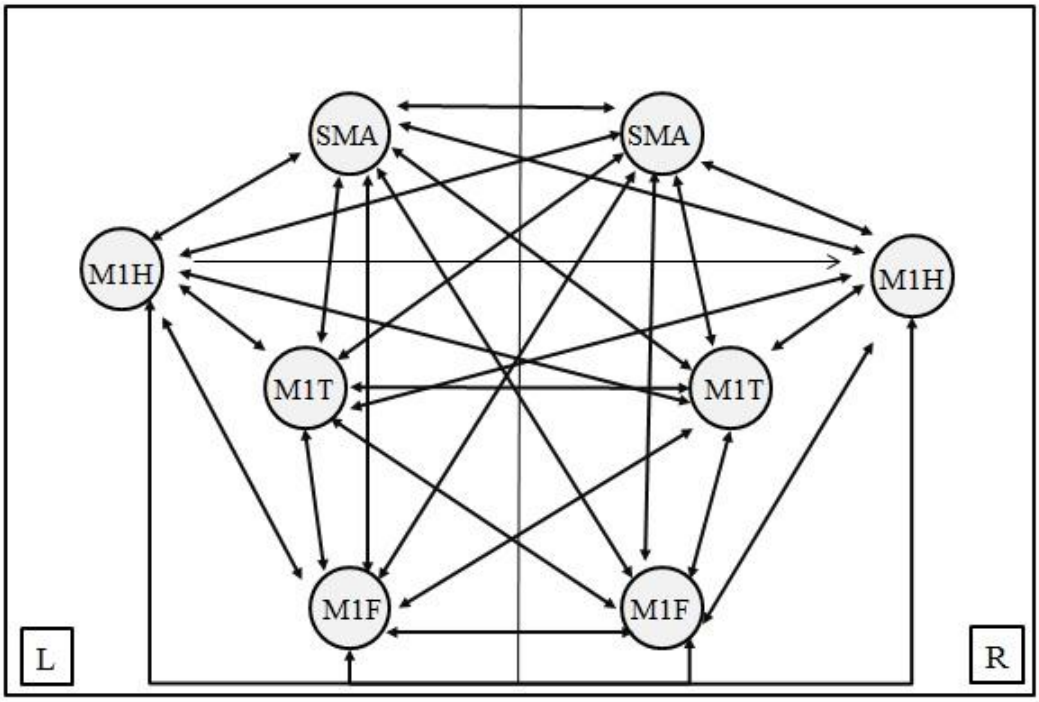

Figure 3.8: Demonstration of Model 4. This model was named as the 'fully-connected model', based on the assumption that the motor task modulates all the connections between the brain regions.

3.3.2.2 Bayesian Model Selection

All four models were estimated and Bayesian model selection (Penny, Stephan, Mechelli, & Friston, 2004) was applied in order to identify the model with the highest evidence (variance explained) given the data using the fixed-effects approach (Penny, 2012; Stephan, Penny, Daunizeau, Moran, & Friston, 2009). The total mean variance explained by the winning model was computed by using the script (spm_dcm_fmri_check.m) provided by Karl Friston in the SPM helpline (2012; https://www.jiscmail.ac.uk/cgi-bin/webadmin?A2=spm;bebd494.1203) (Volz et al., 2015).

3.3.2.3 Bayesian Parameter Averaging

Bayesian Parameter Averaging (BPA) was then applied on the winning model to find the strength of the bidirectional connections. These values provide the insight into the modulation caused by the task on the connections of the regions actively involved during the performance of the task.

Chapter 4

RESULTS AND DISCUSSION

4.1 BOLD activation

The fMRI group analysis (Figure 4.1) revealed that the movement of the right-hand leads to an increased activation of BOLD activity in the left motor network consisting of M1hand (left), bilateral vPMC, SMA, bilateral extrastriate cortex, bilateral striate, as well as subcortical regions including the right anterior cerebellum, left putamen and left thalamus ($p < 0.05$, FWE corrected). Similar, but a mirror reversed pattern of network activation was observed for the movement of the left hand (Figure 4.2). Likewise, foot unilateral movements elicit a similar fashion of activation in premotor, motor and subcortical areas (Figures 4.3 and 4.4). More importantly, each movement resulted in significant activation of the premotor regions, SMA and vPMC, validating that these regions, which we included in our DCM analysis, were actively involved in all the conditions.

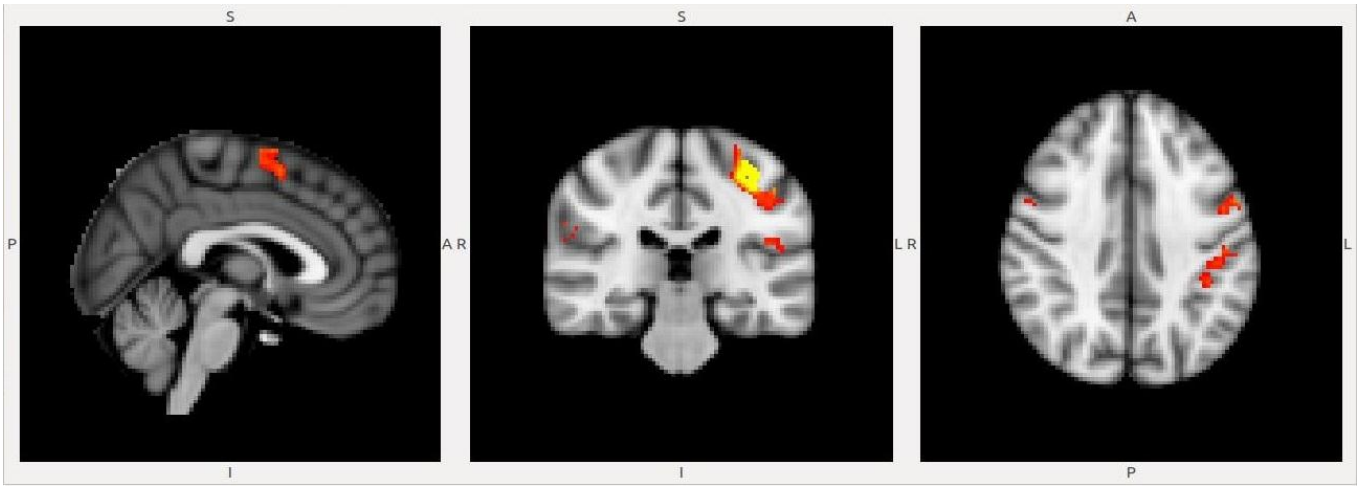

Figure 4.1: Activation map resulting from the movement of the right hand. Prominent activation found at the motor representation of the hand in the left hemisphere (contralateral to the movement) Height threshold: 5.07, $P < 0.05$ (FWE)

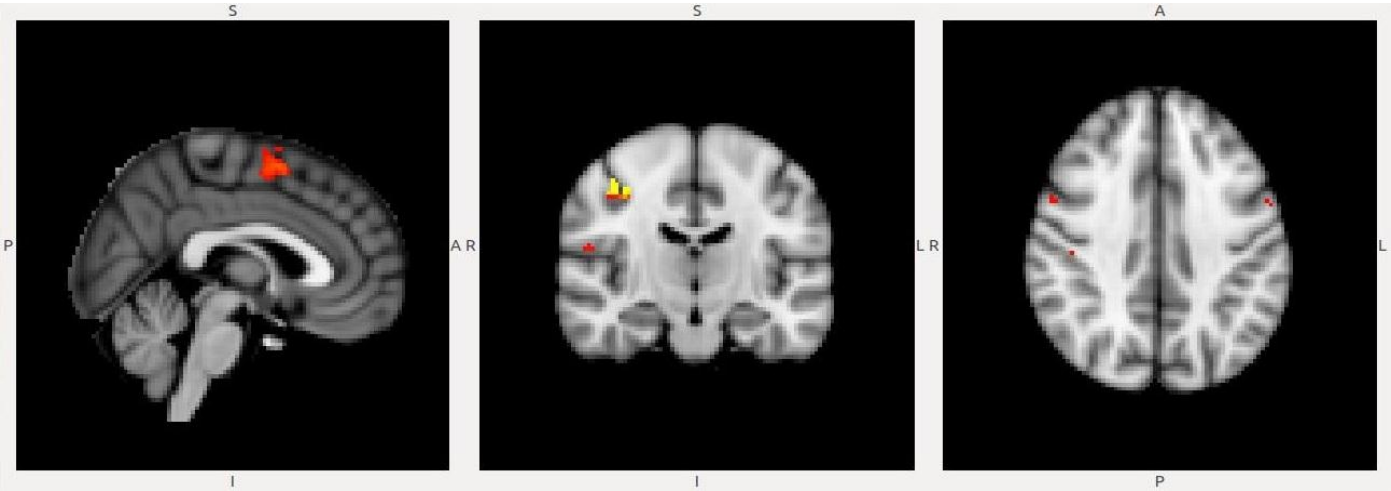

Figure 4.2: Activation map resulting from the movement of the left hand. Prominent activation found at the motor representation of the hand in the right hemisphere (contralateral to the movement) Height threshold: 5.07, $P < 0.05$ (FWE)

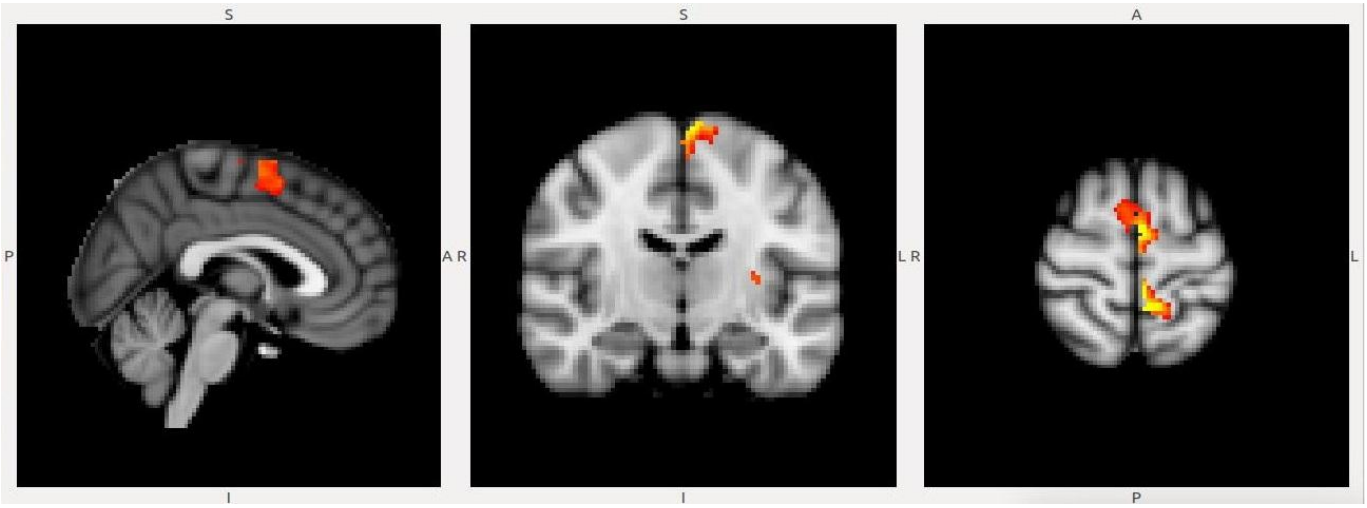

Figure 4.3: Activation map resulting from the movement of the right foot. Prominent activation found at the motor representation of the foot in the left hemisphere (contralateral to the movement) Height threshold: 5.07, $P < 0.05$ (FWE)

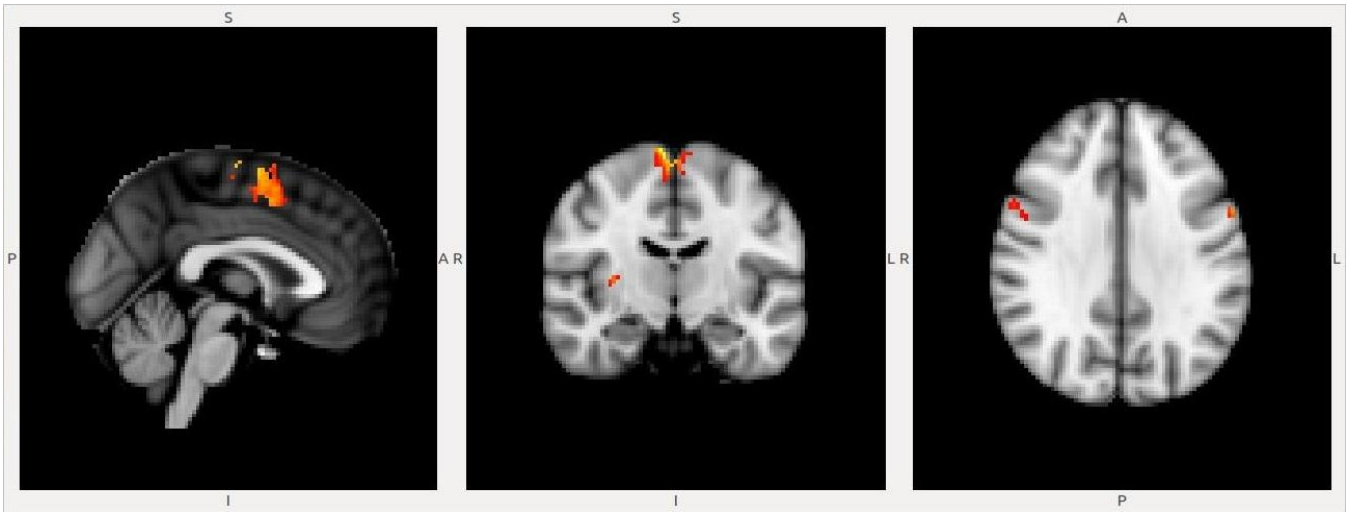

Figure 4.4: Activation map resulting from the movement of the left foot. Prominent activation found at the motor representation of the foot in the right hemisphere (contralateral to the movement) Height threshold: 5.07, $P < 0.05$ (FWE)

4.2 Bayesian model selection

The purpose of model selection is to determine a model, from a set of plausible alternatives, which is most useful, i.e., represents the best balance between accuracy and complexity and thus affords maximal generalizability. The results of the Bayesian model selection applied on all four models at the subject level consistently showed for the subjects (n=20) that Model 3 had the highest value for log evidence (relative) which is showed in Figure 4.5. It was hence regarded as the most generative model of the data. The winning model on average explained 39% of the variance, which represents a good fit of the observed and predicted responses. Of note, model comparison was not based on percentage variance explained by the winning model, but was based on negative free energy which accounts for both the complexity and the model fit (Penny, 2012).

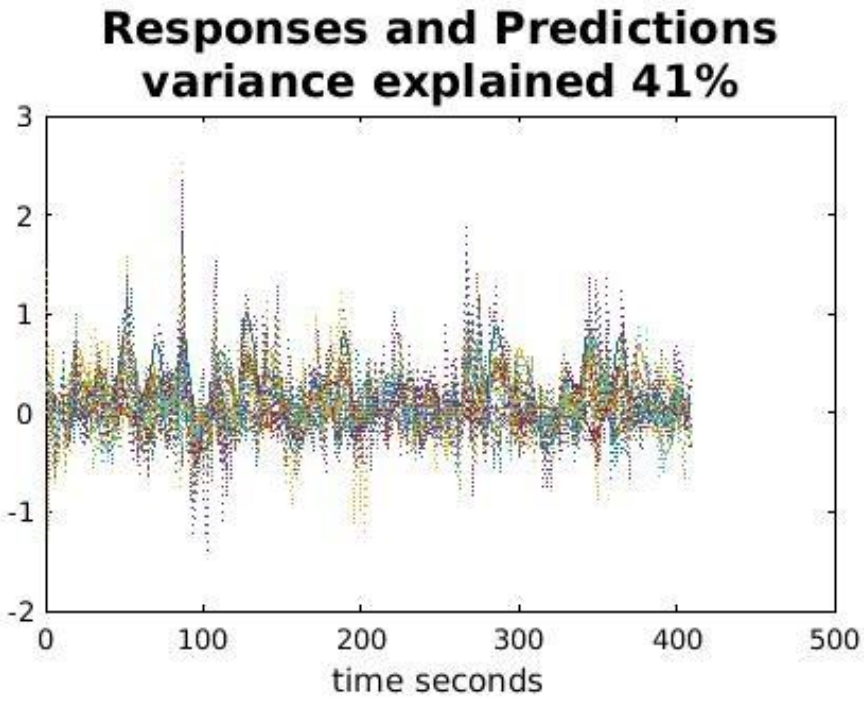

Figure 4.5: Percentage variance explained for the winning model

Table 4.1: Model evidence shown in the form of percentage variance explained for all four models for all subjects (n=20)

Subject No.	M1 Ipsilateral Connections	M2 Contralateral Connections	M3 Self Connections	M4 Fully Connected
01	17%	16%	25%	19%
02	15%	15%	27%	12%
03	17%	16%	38%	15%
04	17%	16%	38%	15%
05	27%	30%	39%	30%
06	21%	22%	35%	22%
07	30%	30%	40%	29%
08	52%	33%	46%	35%
09	24%	28%	33%	25%
10	16%	26%	37%	34%
11	35%	39%	35%	23%
12	24%	14%	29%	13%
13	14%	16%	30%	17%
14	43%	34%	38%	30%
15	29%	29%	42%	34%
16	28%	35%	43%	40%
17	31%	36%	39%	26%
18	28%	25%	37%	45%
19	45%	19%	28%	50%
20	38%	23%	38%	48%

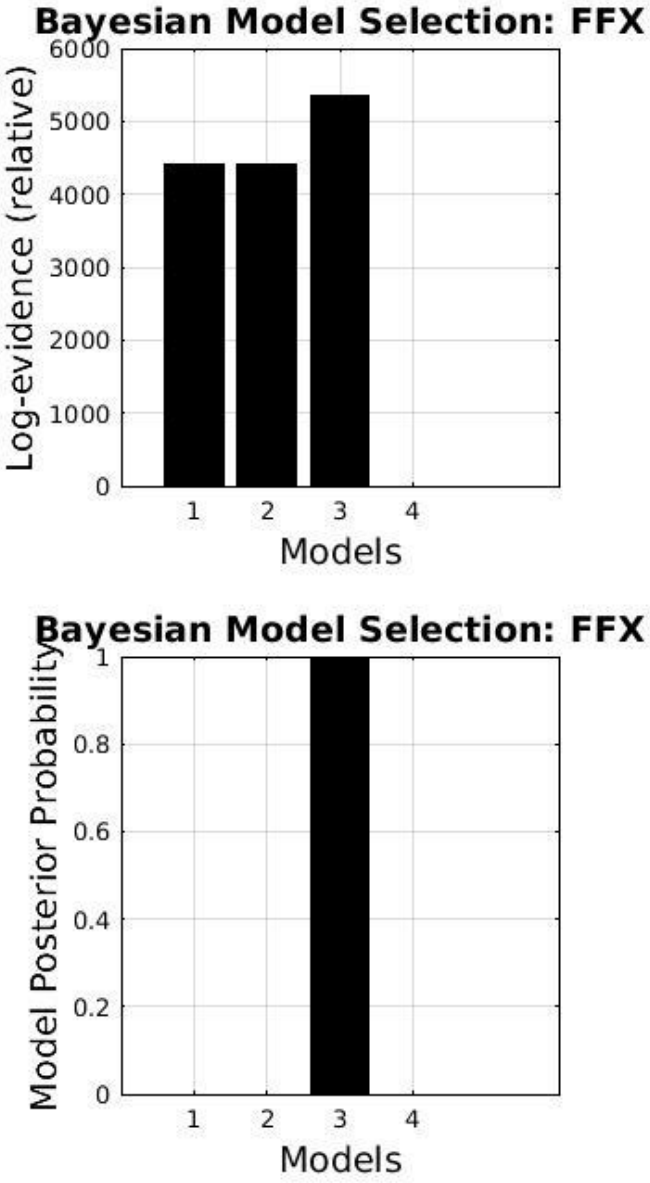

Figure 4.6: Bayesian model selection (BMS) based on fixed effects. Results of BMS applied on all four models using fixed effects show that Model 3 has the highest log evidence and thus is selected as a winning model.

4.3 Tongue-movement specific connectivity

Task specific changes in the neuronal coupling elicited by the movement of the tongue in the motor network are represented in matrix-B (p-value < 0.05, FDR corrected) of the DCM. Figure 4.7 shows the overall neural coupling obtained as a result of Bayesian model averaging. Movement of the tongue was accompanied by enhanced bilateral excitatory input from the SMA onto the left M1tongue. In contrast, the right M1tongue received an excitatory input from the ipsilateral SMA and an inhibitory input from the contralateral SMA (Fig 4.9). Of note, both the right and left SMA exerted significant inhibitory influences onto all the M1 representations of the hands and feet, that is, M1HR, M1HL, M1FR and M1FL (Fig 4.8). Notably, the self-connection of the left M1tongue was strongly inhibited while the self-connection of the right M1tongue was negatively inhibited as shown in Figure 4.10. Lastly, the backward connections from M1TL to the bilateral SMA were excitatory while the backward connections from M1TR to the bilateral SMA were inhibitory as illustrated in Figure 4.11.

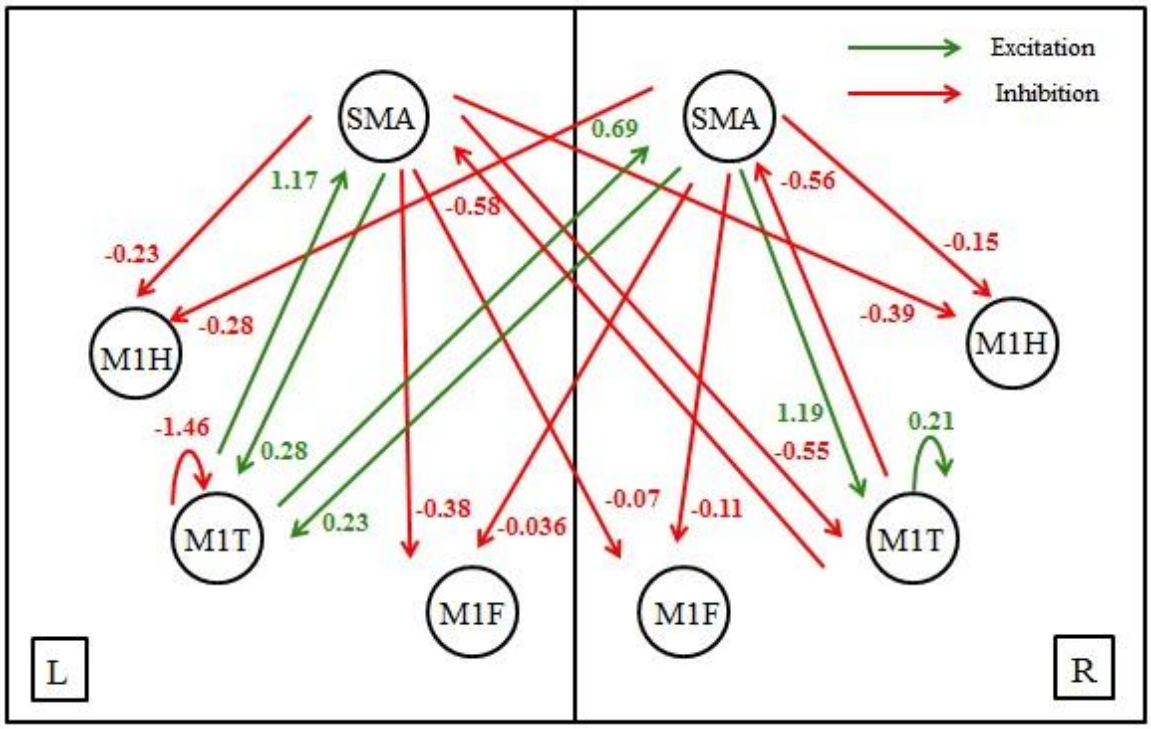

Figure 4.7: Tongue movement specific modulation in motor network. An overview of the results obtained from Bayesian parameter averaging (BPA) applied on the winning model (Model 3).

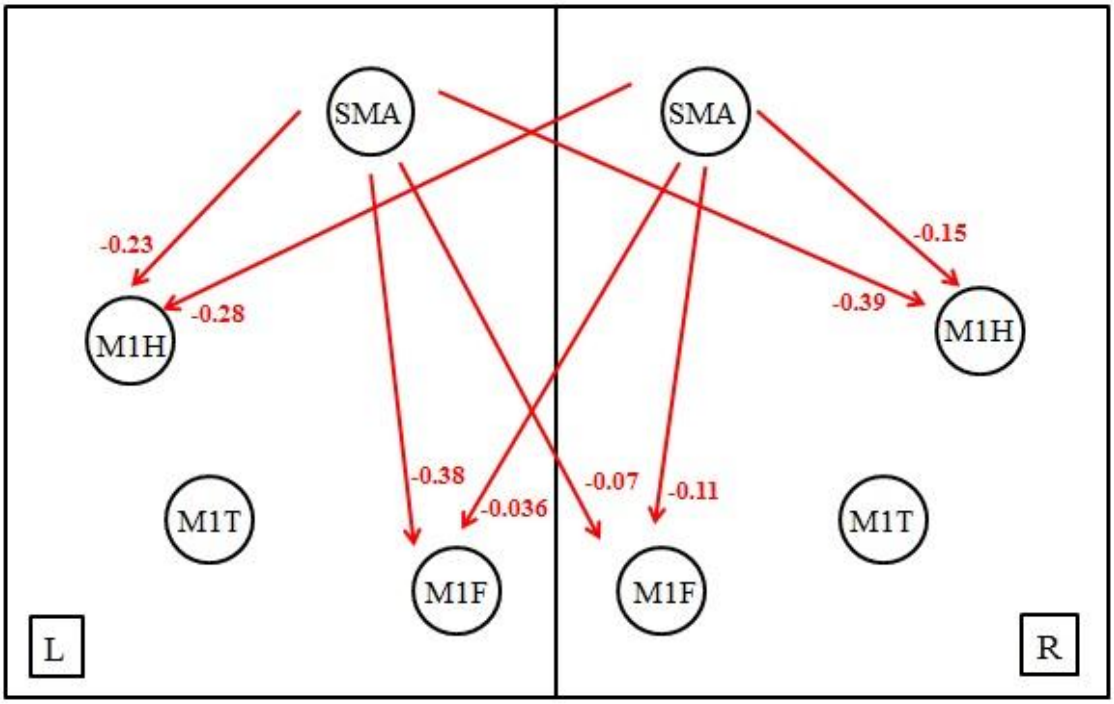

Figure 4.8: The inhibition of M1 representations of the hands and feet by the SMA. BPA results showed movement of the tongue does not differentially facilitate any of the movements of the upper or lower limbs, instead the M1hand and M1foot are equally inhibited by the SMA in both hemispheres.

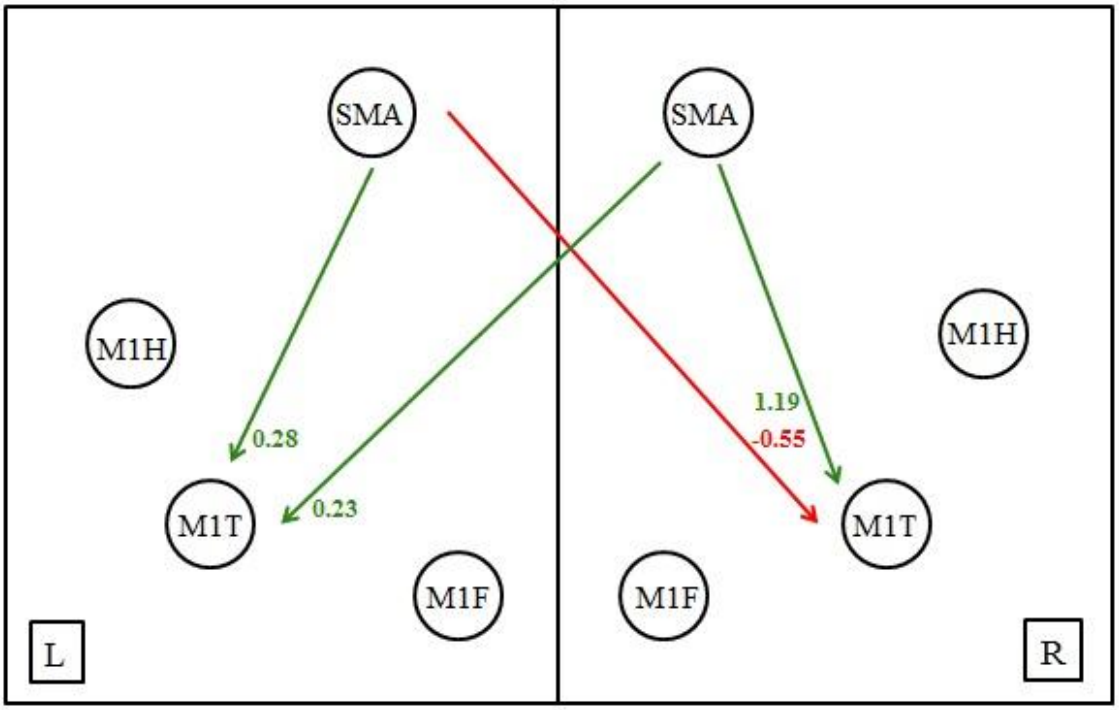

Figure 4.9: Differential influence received by the M1TL and M1TR from the SMA. This illustration shows that the M1TL receives excitatory input from the bilateral SMA while M1TR receives inhibitory input from the contralateral SMA and an excitatory input from the ipsilateral SMA.

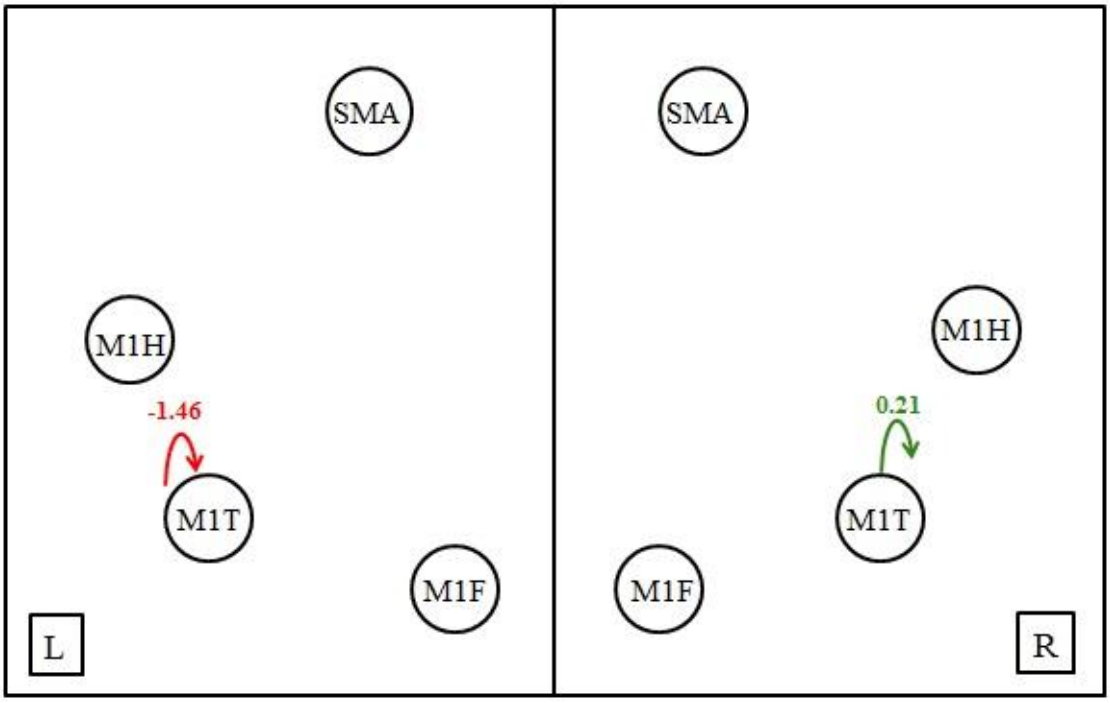

Figure 4.10: Self-connections of the M1tongue. The figure shows that the self-connection of M1TR is inhibitory in nature because it is positive, while the self-connection of M1TL is negative which means that it is excitatory in nature, thus facilitating the movement of the tongue.

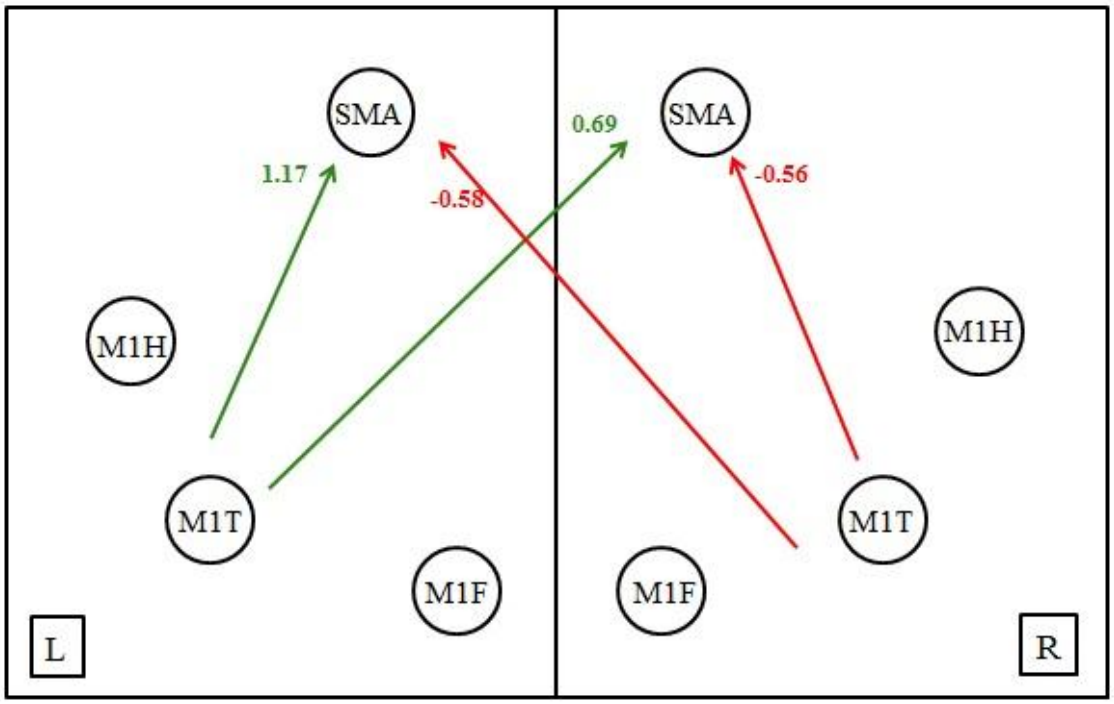

Figure 4.11: Backward connections from M1T to SMA. The backward connections of the M1TL are shown to be positive while the M1TR exerts inhibitory influence onto the bilateral SMA.

4.4 Discussion

The motor network dynamics have not been investigated for tongue movements in the past. This is the first study to assess the modulation of the motor network caused by tongue movements using dynamic causal modeling. DCM is a robust technique which unfolds the patterns of brain connectivity in terms of strength and directionality of connections between different parts of the brain. DCM is a hypothesis driven approach which provides the understanding of how different parts of the brain modulate and influence the activity in each other. We found that the motor network dynamics differ in terms of lateralization when tongue movements are performed. The key finding were the differences in the dynamics of the neural coupling of motor representations of the tongue, reflecting the differential activation profiles of M1TR and M1TL, suggesting left hemispheric lateralization for the movement of the tongue.

There are four aspects which reflect left lateralization of tongue movements based on the inference of model parameters of the winning model of DCM as shown in Figure 4.8.

First, the movement of the tongue does not favor any of the limb movements. M1H and M1F in both the hemispheres receive strong inhibition from the bilateral SMA while the tongue was being moved. This finding suggests that the movement of the hand or foot are not differentially assisted by the M1 representations of the tongue. This is the first study investigating the interaction of the movement of the tongue with the movements of the upper and lower limbs using DCM. Being the first study, it has a few limitations as well. Our winning model did not consist of direct connections between the M1T, M1H and M1F, which limits our analysis to the indirect link of these M1 representations via the SMA. The Bayesian model selection (BMS) is based on the tradeoff between model accuracy and complexity. Further work is required to design more models in terms of the number of connections to explore a more plausible explanation for the data. Furthermore, the number of ROIs, which are eight in our study, also limits our analysis. More robust techniques such as Bayesian model reduction can be applied to automate the designing of multiple models and to finesse the model estimation step, hence making the procedure more robust and computationally feasible.

Second, the M1TL receives bilaterally enhanced excitatory input from both the SMA as compared to M1TR, which received pronounced inhibitory input from the contralateral SMA and excitatory input from the ipsilateral SMA (Fig 4.9). Thirdly, the backward connections, that is from the M1tongue to the SMA show a distinct pattern in terms of lateralization (Fig 4.11). The M1TL exerts a strong excitatory drive onto both SMA. In stark contrast, M1TR exerts a strong inhibition onto the bilateral SMA. Lastly, the self-connections of the M1TL and M1TR show

interesting results. The M1TR was found to be strongly inhibited while the tongue was being moved, while the M1TL was weakly inhibited (or excited) relatively as illustrated in Figure 4.10.

Our DCM results are consistent with previous fMRI studies reporting lateralization of tongue movement (Funk et al., 2008; Hesselmann et al., 2004; Martin et al., 2004). While other groups did not observe significant inter-hemispheric differences and thus have concluded motor representation of the tongue to be symmetric, when movements of the tongue were executed (Corfield et al., 1999; Fesl et al., 2003; Wildgruber, Ackermann, Klose, Kardatzki, & Grodd, 1996). These contradicting hypotheses may have occurred due to slight changes in the task performance and types of analysis. Some of the studies investigated vertical movements of the tongue while others have focused on horizontal tongue movements. Secondly, most of the previous results are based on the activated cluster size which is the volume of activation and not on the intensity of the activated cluster. A standard lateralization tool should be used to investigate and compare such hypotheses. Also, more advanced techniques such as DCM, other than just functional connectivity analysis, should be applied to explore such lateralization of brain functions. Furthermore, handedness could be a good measure of investigating the behavioral asymmetry of the tongue. There are no studies reported on the motor tongue lateralization and its link to the handedness. Studies have reported indirect links between handedness and tongue lateralization based on chewing side preference (Nissan, Gross, Shifman, Tzadok, & Assif, 2004; Shinagawa et al., 2004; Shinagawa et al., 2003), suggesting that a link may exist between tongue dominance behavior and handedness.

Chapter 5

CONCLUSION & FUTURE RECOMMENDATIONS

5.1 Conclusion

Our results show differential activation profiles of the right and left M1 representations of the tongue (M1TR & M1TL) suggesting the motor control of the tongue to be left lateralized. Regardless of the similar organization of connections, the M1TL was found to be associated with stronger coupling with the SMA. Our DCM results are consistent with previous fMRI studies reporting lateralization of tongue movement. We also found that the tongue movement does not differentially facilitate any of the upper or lower limb movements; instead the SMA equally inhibits both the M1 representations of the hand (M1hand) and the foot (M1foot).

5.2 Future Recommendations

As this is the first study investigating the lateralized motor control of tongue and the association of movement of the tongue with the movement of the hands and feet using dynamic causal modeling, the analysis can be improved by overcoming some of the limitations. The future perspectives are as follows:

1. The model space, which is the number of brain regions, included in this study was eight, which limits our evaluation for any plausible models practically impossible. For a small number of regions, it is possible to investigate all the possible connections, by constructing several plausible models. Hence, reducing the number of regions by defining the hypothesis more precisely, we can make the analysis more efficient in terms of computational power as well

as the interpretation of results. That way we can design multiple plausible models exploring more parameters in terms of brain connections.

2. We investigated four models to explain our data. Our winning model consisted of indirect links between the motor representations of the tongue with the upper and lower limbs, via the SMA. However, the SMA is an important constituent of the motor network, being involved in assisting and supplementing the movements, but our analysis remains indirect and dependent on the SMA connections to the tongue and the limb region. More conclusive results can be made if we improve our model parameters by constructing multiple plausible models, which links this recommendation to the above. By decreasing the number regions (model space), we can increase the number of models explaining the data.

3. Other premotor regions can be added to the motor network to improve the analysis, such as the ventral premotor cortex (vPMC) which is involved in the transformations of the sensory-motor information.

4. Techniques such as Bayesian model reduction can be applied to finesse the estimation of multiple models, therefore making the analysis robust and computationally feasible.

5. We have investigated the lateralization of the tongue using group level analysis of functional connectivity data and DCM. Behavioral data such as handedness can be incorporated into the study to explore the behavioral asymmetry of the tongue.

Chapter 6

REFERENCES

Boudrias, M. H., Goncalves, C. S., Penny, W. D., Park, C. H., Rossiter, H. E., Talelli, P., & Ward, N. S. (2012). Age-related changes in causal interactions between cortical motor regions during hand grip. *Neuroimage, 59*(4), 3398-3405. doi: 10.1016/j.neuroimage.2011.11.025

Boussaoud, D., Tanne-Gariepy, J., Wannier, T., & Rouiller, E. M. (2005). Callosal connections of dorsal versus ventral premotor areas in the macaque monkey: a multiple retrograde tracing study. *BMC Neurosci, 6*, 67. doi: 10.1186/1471-2202-6-67

Buckner, R. L., Krienen, F. M., Castellanos, A., Diaz, J. C., & Yeo, B. T. (2011). The organization of the human cerebellum estimated by intrinsic functional connectivity. *J Neurophysiol, 106*(5), 2322-2345. doi: 10.1152/jn.00339.2011

Corfield, D. R., Murphy, K., Josephs, O., Fink, G. R., Frackowiak, R. S., Guz, A., . . . Turner, R. (1999). Cortical and subcortical control of tongue movement in humans: a functional neuroimaging study using fMRI. *J Appl Physiol (1985), 86*(5), 1468-1477. doi: 10.1152/jappl.1999.86.5.1468

Dirnagl, U., Niwa, K., Lindauer, U., & Villringer, A. (1994). Coupling of cerebral blood flow to neuronal activation: role of adenosine and nitric oxide. *Am J Physiol, 267*(1 Pt 2), H296-301.

Duncan, G. E., & Stumpf, W. E. (1991). Brain activity patterns: assessment by high resolution autoradiographic imaging of radiolabeled 2-deoxyglucose and glucose uptake. *Prog Neurobiol, 37*(4), 365-382.

Duncan, G. E., Stumpf, W. E., & Pilgrim, C. (1987). Cerebral metabolic mapping at the cellular level with dry-mount autoradiography of [3H]2-deoxyglucose. *Brain Res, 401*(1), 43-49.

Eickhoff, S. B., & Grefkes, C. (2011). Approaches for the integrated analysis of structure, function and connectivity of the human brain. *Clin EEG Neurosci, 42*(2), 107-121. doi: 10.1177/155005941104200211

Fesl, G., Moriggl, B., Schmid, U. D., Naidich, T. P., Herholz, K., & Yousry, T. A. (2003). Inferior central sulcus: variations of anatomy and function on the example of the motor tongue area. *Neuroimage, 20*(1), 601-610.

Friston, K. J. (2011). Functional and effective connectivity: a review. *Brain Connect, 1*(1), 13-36. doi: 10.1089/brain.2011.0008

Friston, K. J., Harrison, L., & Penny, W. (2003). Dynamic causal modelling. *Neuroimage, 19*(4), 1273-1302.

Funk, M., Lutz, K., Hotz-Boendermaker, S., Roos, M., Summers, P., Brugger, P., . . . Kollias, S. S. (2008). Sensorimotor tongue representation in individuals with unilateral upper limb amelia. *Neuroimage, 43*(1), 121-127. doi: 10.1016/j.neuroimage.2008.06.011

Gjedde, Albert. (1997). The relation between brain function and cerebral blood flow and metabolism. *Cerebrovascular disease,* 23-40.

Glasser, M. F., Sotiropoulos, S. N., Wilson, J. A., Coalson, T. S., Fischl, B., Andersson, J. L., . . . Consortium, W. U-Minn HCP. (2013). The minimal preprocessing pipelines for the Human Connectome Project. *Neuroimage, 80,* 105-124. doi: 10.1016/j.neuroimage.2013.04.127

Glendenning, K. K., Hutson, K. A., Nudo, R. J., & Masterton, R. B. (1985). Acoustic chiasm II: Anatomical basis of binaurality in lateral superior olive of cat. *J Comp Neurol, 232*(2), 261-285. doi: 10.1002/cne.902320210

Grafton, S. T., Woods, R. P., & Mazziotta, J. C. (1993). Within-arm somatotopy in human motor areas determined by positron emission tomography imaging of cerebral blood flow. *Exp Brain Res, 95*(1), 172-176.

Grefkes, C., Eickhoff, S. B., Nowak, D. A., Dafotakis, M., & Fink, G. R. (2008). Dynamic intra- and interhemispheric interactions during unilateral and bilateral hand movements assessed with fMRI and DCM. *Neuroimage, 41*(4), 1382-1394. doi: 10.1016/j.neuroimage.2008.03.048

Hesselmann, V., Sorger, B., Lasek, K., Guntinas-Lichius, O., Krug, B., Sturm, V., . . . Lackner, K. (2004). Discriminating the cortical representation sites of tongue and up movement by functional MRI. *Brain Topogr, 16*(3), 159-167.

Hock, C., Muller-Spahn, F., Schuh-Hofer, S., Hofmann, M., Dirnagl, U., & Villringer, A. (1995). Age dependency of changes in cerebral hemoglobin oxygenation during brain activation: a near-infrared spectroscopy study. *J Cereb Blood Flow Metab, 15*(6), 1103-1108. doi: 10.1038/jcbfm.1995.137

Kapreli, E., Athanasopoulos, S., Papathanasiou, M., Van Hecke, P., Strimpakos, N., Gouliamos, A., . . . Sunaert, S. (2006). Lateralization of brain activity during lower limb joints movement. An fMRI study. *Neuroimage, 32*(4), 1709-1721. doi: 10.1016/j.neuroimage.2006.05.043

Kuschinsky, W. (1991). Coupling of function, metabolism, and blood flow in the brain. *Neurosurg Rev, 14*(3), 163-168.

Logothetis, N. K. (2008). What we can do and what we cannot do with fMRI. *Nature, 453*(7197), 869-878. doi: 10.1038/nature06976

Lotze, M., Seggewies, G., Erb, M., Grodd, W., & Birbaumer, N. (2000). The representation of articulation in the primary sensorimotor cortex. *Neuroreport, 11*(13), 2985-2989.

Luft, A. R., Smith, G. V., Forrester, L., Whitall, J., Macko, R. F., Hauser, T. K., . . . Hanley, D. F. (2002). Comparing brain activation associated with isolated upper and lower limb movement across corresponding joints. *Hum Brain Mapp, 17*(2), 131-140. doi: 10.1002/hbm.10058

Luppino, G., Matelli, M., Camarda, R., & Rizzolatti, G. (1993). Corticocortical connections of area F3 (SMA-proper) and area F6 (pre-SMA) in the macaque monkey. *J Comp Neurol, 338*(1), 114-140. doi: 10.1002/cne.903380109

Magistretti, P. J., & Pellerin, L. (1996). The contribution of astrocytes to the 18F-2-deoxyglucose signal in PET activation studies. *Mol Psychiatry, 1*(6), 445-452.

Mansfield, Peter. (1977). Multi-planar image formation using NMR spin echoes. *Journal of Physics C: Solid State Physics, 10*(3), L55.

Marquart, M., Birn, R., & Haughton, V. (2000). Single- and multiple-event paradigms for identification of motor cortex activation. *AJNR Am J Neuroradiol, 21*(1), 94-98.

Martin, R. E., MacIntosh, B. J., Smith, R. C., Barr, A. M., Stevens, T. K., Gati, J. S., & Menon, R. S. (2004). Cerebral areas processing swallowing and tongue movement are overlapping but distinct: a functional magnetic resonance imaging study. *J Neurophysiol, 92*(4), 2428-2443. doi: 10.1152/jn.01144.2003

Mathiesen, C., Caesar, K., Akgoren, N., & Lauritzen, M. (1998). Modification of activity-dependent increases of cerebral blood flow by excitatory synaptic activity and spikes in rat cerebellar cortex. *J Physiol, 512 (Pt 2)*, 555-566.

McGuire, P. K., Bates, J. F., & Goldman-Rakic, P. S. (1991). Interhemispheric integration: I. Symmetry and convergence of the corticocortical connections of the left and the right principal sulcus (PS) and the left and the right supplementary motor area (SMA) in the rhesus monkey. *Cereb Cortex, 1*(5), 390-407.

Meek, J. H., Firbank, M., Elwell, C. E., Atkinson, J., Braddick, O., & Wyatt, J. S. (1998). Regional hemodynamic responses to visual stimulation in awake infants. *Pediatr Res, 43*(6), 840-843. doi: 10.1203/00006450-199806000-00019

Nissan, J., Gross, M. D., Shifman, A., Tzadok, L., & Assif, D. (2004). Chewing side preference as a type of hemispheric laterality. *J Oral Rehabil, 31*(5), 412-416. doi: 10.1111/j.1365-2842.2004.01256.x

Ogawa, S., Lee, T. M., Kay, A. R., & Tank, D. W. (1990). Brain magnetic resonance imaging with contrast dependent on blood oxygenation. *Proc Natl Acad Sci U S A, 87*(24), 9868-9872.

Ogawa, S., Menon, R. S., Tank, D. W., Kim, S. G., Merkle, H., Ellermann, J. M., & Ugurbil, K. (1993). Functional brain mapping by blood oxygenation level-dependent contrast magnetic resonance imaging. A comparison of signal characteristics with a biophysical model. *Biophys J, 64*(3), 803-812. doi: 10.1016/S0006-3495(93)81441-3

Ogawa, Seiji, & Lee, Tso-Ming. (1990). Magnetic resonance imaging of blood vessels at high fields: in vivo and in vitro measurements and image simulation. *Magnetic resonance in medicine, 16*(1), 9-18.

Ogawa, Seiji, Lee, Tso-Ming, Nayak, Asha S, & Glynn, Paul. (1990). Oxygenation-sensitive contrast in magnetic resonance image of rodent brain at high magnetic fields. *Magnetic resonance in medicine, 14*(1), 68-78.

Pauling, L., & Coryell, C. D. (1936). The Magnetic Properties and Structure of Hemoglobin, Oxyhemoglobin and Carbonmonoxyhemoglobin. *Proc Natl Acad Sci U S A, 22*(4), 210-216.

Penfield, Wilder, & Boldrey, Edwin. (1937). Somatic motor and sensory representation in the cerebral cortex of man as studied by electrical stimulation. *Brain, 60*(4), 389-443.

Penny, W. D. (2012). Comparing dynamic causal models using AIC, BIC and free energy. *Neuroimage, 59*(1), 319-330. doi: 10.1016/j.neuroimage.2011.07.039

Penny, W. D., Stephan, K. E., Mechelli, A., & Friston, K. J. (2004). Comparing dynamic causal models. *Neuroimage, 22*(3), 1157-1172. doi: 10.1016/j.neuroimage.2004.03.026

Peter Jezzard, Paul M. Matthews, and Stephen M. Smith. (2003). *Functional MRI: An Introduction to Methods* (1 ed.). USA: Oxford University Press.

Rees, G., Friston, K., & Koch, C. (2000). A direct quantitative relationship between the functional properties of human and macaque V5. *Nat Neurosci, 3*(7), 716-723. doi: 10.1038/76673

Rouiller, E. M., Babalian, A., Kazennikov, O., Moret, V., Yu, X. H., & Wiesendanger, M. (1994). Transcallosal connections of the distal forelimb representations of the primary and supplementary motor cortical areas in macaque monkeys. *Exp Brain Res, 102*(2), 227-243.

Shinagawa, H., Ono, T., Honda, E., Sasaki, T., Taira, M., Iriki, A., . . . Ohyama, K. (2004). Chewing-side preference is involved in differential cortical activation patterns during tongue movements after bilateral gum-chewing: a functional magnetic resonance imaging study. *J Dent Res, 83*(10), 762-766. doi: 10.1177/154405910408301005

Shinagawa, H., Ono, T., Ishiwata, Y., Honda, E., Sasaki, T., Taira, M., . . . Kuroda, T. (2003). Hemispheric dominance of tongue control depends on the chewing-side preference. *J Dent Res, 82*(4), 278-283. doi: 10.1177/154405910308200407

Sibson, N. R., Dhankhar, A., Mason, G. F., Rothman, D. L., Behar, K. L., & Shulman, R. G. (1998). Stoichiometric coupling of brain glucose metabolism and glutamatergic neuronal activity. *Proc Natl Acad Sci U S A, 95*(1), 316-321.

Stephan, K. E., Penny, W. D., Daunizeau, J., Moran, R. J., & Friston, K. J. (2009). Bayesian model selection for group studies. *Neuroimage, 46*(4), 1004-1017. doi: 10.1016/j.neuroimage.2009.03.025

Thulborn, K. R., Waterton, J. C., Matthews, P. M., & Radda, G. K. (1982). Oxygenation dependence of the transverse relaxation time of water protons in whole blood at high field. *Biochim Biophys Acta, 714*(2), 265-270.

Van Essen, D. C., Smith, S. M., Barch, D. M., Behrens, T. E., Yacoub, E., Ugurbil, K., & Consortium, W. U-Minn HCP. (2013). The WU-Minn Human Connectome Project: an overview. *Neuroimage, 80*, 62-79. doi: 10.1016/j.neuroimage.2013.05.041

Van Essen, D. C., Ugurbil, K., Auerbach, E., Barch, D., Behrens, T. E., Bucholz, R., . . . Consortium, W. U-Minn HCP. (2012). The Human Connectome Project: a data acquisition perspective. *Neuroimage, 62*(4), 2222-2231. doi: 10.1016/j.neuroimage.2012.02.018

Volz, L. J., Eickhoff, S. B., Pool, E. M., Fink, G. R., & Grefkes, C. (2015). Differential modulation of motor network connectivity during movements of the upper and lower limbs. *Neuroimage, 119*, 44-53. doi: 10.1016/j.neuroimage.2015.05.101

Wang, L. E., Fink, G. R., Diekhoff, S., Rehme, A. K., Eickhoff, S. B., & Grefkes, C. (2011). Noradrenergic enhancement improves motor network connectivity in stroke patients. *Ann Neurol, 69*(2), 375-388. doi: 10.1002/ana.22237

Wildgruber, D., Ackermann, H., Klose, U., Kardatzki, B., & Grodd, W. (1996). Functional lateralization of speech production at primary motor cortex: a fMRI study. *Neuroreport, 7*(15-17), 2791-2795.

Yeo, B. T., Krienen, F. M., Sepulcre, J., Sabuncu, M. R., Lashkari, D., Hollinshead, M., . . . Buckner, R. L. (2011). The organization of the human cerebral cortex estimated by intrinsic functional connectivity. *J Neurophysiol*, *106*(3), 1125-1165. doi: 10.1152/jn.00338.2011